LIFE SCIENCES

Nonredundancy of IL-1α and IL-1β is defined by distinct regulation of tissues orchestrating resistance versus tolerance to infection

Kevin Eislmayr[1], Annika Bestehorn[1], Luisa Morelli[1], Martina Borroni[1], Lieselotte Vande Walle[2], Mohamed Lamkanfi[2], Pavel Kovarik[1]*

Interleukin-1α (IL-1α) and IL-1β are inflammatory cytokines with important roles in health and disease. They trigger the same receptor and elicit comparable cellular responses but, for poorly understood reasons, are not redundant in vivo. Here, we decoupled IL-1α and IL-1β functions that drive protective responses against invasive infection with group A *Streptococcus*. IL-1β was essential for pathogen clearance, hence resistance to infection, by inducing granulocyte colony-stimulating factor at the infection site and establishing emergency granulopoiesis. In contrast, IL-1α governed reprogramming of liver metabolic pathways associated with tolerance to infection. The IL-1α–dominated hepatic regulation corresponded to high IL-1α levels in the liver during infection. Conversely, IL-1β was critical for the regulation of the spleen transcriptome, which correlated with ample IL-1β expression in this tissue. The results identify distinct and organ-specific roles of IL-1α versus IL-1β and implicate spatial restriction of their expression and bioavailability during infection as the underlying mechanism.

INTRODUCTION

Interleukin-1 (IL-1) signaling is one of the most potent triggers and amplifiers of inflammatory responses; it regulates basic physiological processes including defense against infections, metabolism, and tissue homeostasis (*1*, *2*). Conversely, dysregulated IL-1 signaling is involved in pathologies ranging from infectious disease to autoimmune disorders and cancer. It is well established that the activators of IL-1 signaling are the cytokines IL-1α and IL-1β. Given the broad importance of these cytokines, it is unexpected that their distinct functions and the mechanisms underlying their nonredundancy remain poorly defined (*1*, *2*).

IL-1α and IL-1β are encoded by the *Il1a* and *Il1b* genes, respectively, located on chromosome 2 in both humans and mice (*3*). The evolutionarily conserved occurrence of *Il1a* and *Il1b* genes in mammals suggests that these cytokines accomplish nonredundant functions in the mammalian immune system. IL-1α and IL-1β display a limited amino acid sequence similarity but adopt a conserved structure consisting of 12 antiparallel β strands that are arranged in a β barrel core motif (*4*). This structural similarity enables both IL-1α and IL-1β to bind and activate the same receptor, i.e., the IL-1 receptor composed of IL-1R1 and IL-1R3; IL-1α and IL-1β are the only known IL-1R1 agonists. IL-1α and IL-1β appear to generate the same response in the target cell: The ligated IL-1 receptor triggers a myeloid differentiation primary response 88 (Myd88)-dependent signaling cascade that culminates in the activation of mitogen-activated protein (MAP) kinases and several transcription factors, nuclear factor κB (NF-κB), and subsequent gene expression changes (*3*, *5*).

The production of IL-1α and IL-1β is precisely regulated at multiple levels, and dysregulation of IL-1α and IL-1β has been associated with human diseases (*1*). Both *Il1a* and *Il1b* genes are transcriptionally activated by stress and inflammatory stimuli (*6*, *7*). The transcription factors NF-κB, Sp1, and activating protein 1 were shown to activate the Il1a gene (*7*–*10*). The transcriptional regulation of *Il1b* appears to be more complex as both activators such as NF-κB and hypoxia-inducible factor 1α as well as repressors including signal transducers and activators of transcription 1 and natural antisense *Il1b* RNA (*Il1bas*) are involved (*11*–*14*). Another important layer of control of IL-1 production is by means of changes in *Il1a* and *Il1b* mRNA stability (*15*). The bioavailability of IL-1β is critically regulated by posttranslational processing and release from cells (*16*, *17*). The importance of posttranslational regulation is less well explored for IL-1α, which is known to be biologically active both in unprocessed and processed forms (*18*).

Common versus unique effects of *Il1a* and *Il1b* genes in physiological and pathological settings have been addressed in a direct comparison only in few studies. The establishment of gene-targeted mice revealed that *Il1a*-deficient and wild-type (WT) mice develop fever and induce acute phase proteins upon subcutaneous turpentine administration, while *Il1b*-deficient mice lack such responses (*19*). This study suggested that *Il1b* plays a more important role in this sterile inflammation model. In contrast, lipopolysaccharide (LPS)/D-galactosamine–induced fulminant hepatitis failure (FHF) was similarly reduced in *Il1a*- and *Il1b*-deficient mice indicating important functions of both cytokines in FHF (*20*). Opposing effects of *Il1a* and *Il1b* on disease progression were reported in a dextran sulfate–induced colon inflammation model: *Il1a* deficiency resulted in a milder disease, while *Il1b* deficiency correlated with exacerbated conditions (*21*). Both *Il1a* and *Il1b* were found to nonredundantly drive host defense by limiting the growth of *Mycobacterium tuberculosis* in a lung infection model (*22*). In a model of lung infection with *Legionella pneumophila*, *Il1a* was the major player in neutrophil recruitment early in the infection, while *Il1b* was important in the later phase of the infection (*23*). Together, these studies indicate that *Il1a* and *Il1b* have nonredundant functions in sterile and bacterial-mediated inflammation; the mechanisms underlying these distinct effects remain poorly defined. It is also unclear how *Il1a* and *Il1b*

[1]Max Perutz Labs, University of Vienna, Vienna Biocenter (VBC), Dr. Bohr-Gasse 9, A-1030 Vienna, Austria. [2]Laboratory of Medical Immunology, Department of Internal Medicine and Pediatrics, Ghent University, C. Heymanslaan 10, 9000 Ghent, Belgium.
*Corresponding author. Email: pavel.kovarik@univie.ac.at

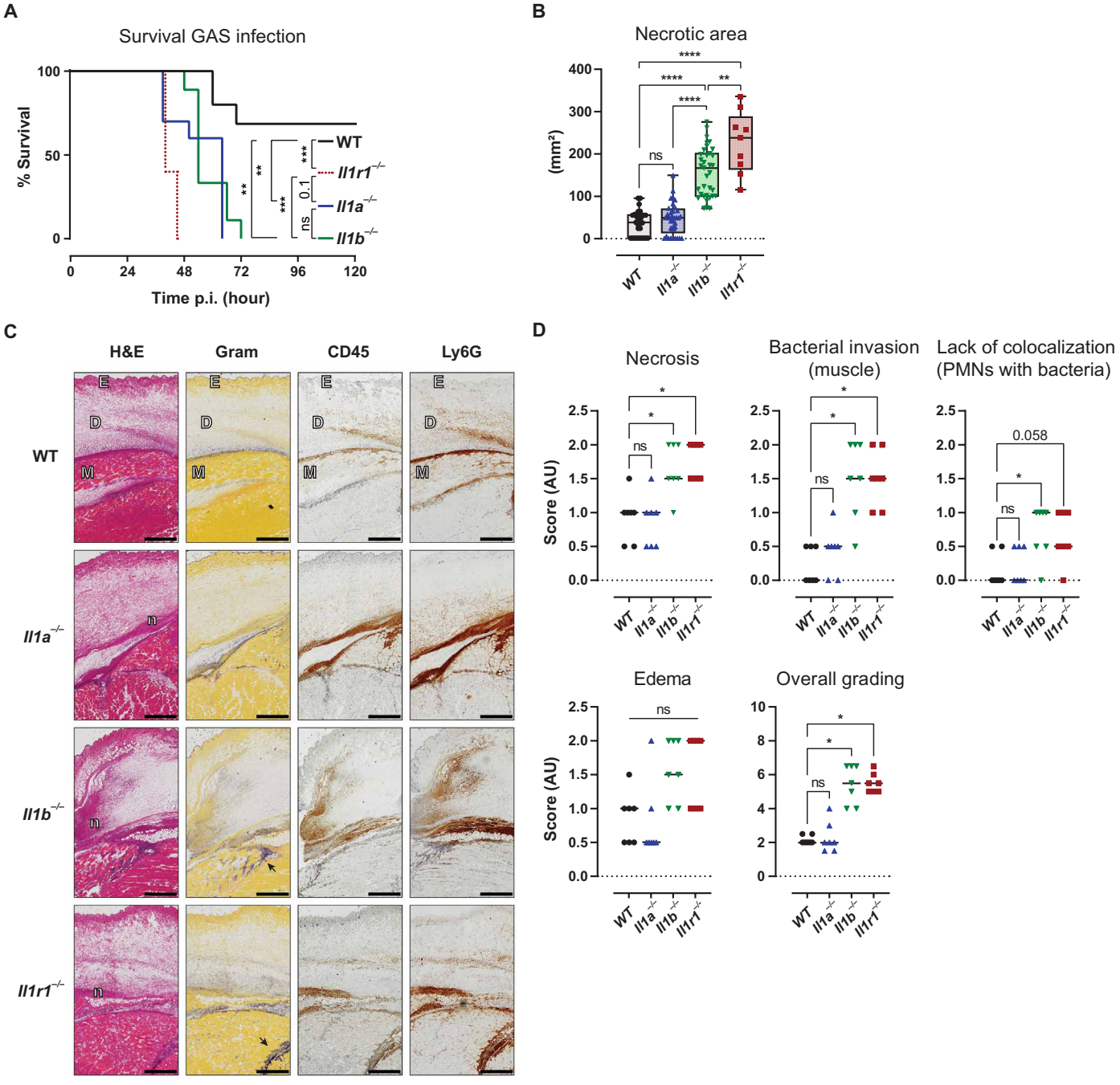

Fig. 1. *Il1a* and *Il1b* are both critical for host protection against GAS. (**A**) Kaplan-Meier survival curves of *Il1a*$^{-/-}$, *Il1b*$^{-/-}$, *Il1r1*$^{-/-}$, and WT mice ($n = 10$ per genotype) subcutaneously infected with GAS [2×10^8 colony-forming units (CFU)]. *Il1a*$^{-/-}$, *Il1b*$^{-/-}$, and *Il1r1*$^{-/-}$ mice were significantly more susceptible than WT mice. The difference between *Il1a*$^{-/-}$ and *Il1b*$^{-/-}$ was not significant. Log-rank Mantel-Cox test with Bonferroni correction for multiple comparison. $^{**}P < 0.01$; $^{***}P < 0.001$. ns, not significant. (**B**) Size of necrotic area at the site of infection in *Il1a*$^{-/-}$, *Il1b*$^{-/-}$, *Il1r1*$^{-/-}$, and WT mice 48 hours p.i. ($n = 35$ for each *WT*, *Il1a*$^{-/-}$, and *Il1b*$^{-/-}$ and $n = 9$ for *Il1r1*$^{-/-}$). Data represent pools of three independent experiments. Box-and-whisker plots with the median value and 10th to 90th percentile. Kruskal-Wallis with Dunn's multiple comparisons test. $^{**}P < 0.01$; $^{****}P < 0.0001$. (**C**) Hematoxylin and eosin (H&E), Gram, CD45, and Ly6G staining of skin sections showing epidermis (E), dermis (D), and muscle (M) from infected *Il1a*$^{-/-}$, *Il1b*$^{-/-}$, *Il1r1*$^{-/-}$, and WT mice 24 hours p.i. H&E staining indicates severe acute necrotizing cellulitis and panniculitis in all sections. Necrotic area (n) is more pronounced in *Il1b*$^{-/-}$ as well as in *Il1r1*$^{-/-}$ mice and range from the dermis into the muscular layer. Gram staining visualizes invasion of tissue with GAS (blue). Note that bacteria show invasion (arrows) of the muscular layer in *Il1b*$^{-/-}$ and *Il1r1*$^{-/-}$ mice but not in *Il1a*$^{-/-}$ and WT mice. Bacteria (Gram) and neutrophils (Ly6G) often do not colocalize in *Il1b*$^{-/-}$ and *Il1r1*$^{-/-}$ samples. Scale bars, 500 μm. (**D**) Quantification of tissue destruction based on staining shown in (C). Parameters used for grading were necrosis, bacterial invasion into the muscular layer, missing colocalization of polymorphonuclear cells (PMNs as Ly6G$^+$) with bacteria, edema, and the overall score [in arbitrary units (AU)] as the sum of all categories. Kruskal-Wallis with Dunn's multiple comparisons test, $n = 7$ per genotype. $^*P < 0.05$.

accomplish their nonoverlapping functions despite eliciting comparable responses in cells.

Here, we report that *Il1a* and *Il1b* drive host defense against severe subcutaneous infection with group A *Streptococcus* (GAS) in nonredundant and mechanistically distinct ways. Using $Il1a^{-/-}$ and $Il1b^{-/-}$ mice, we show that both *Il1a* and *Il1b* are indispensable for a protective defense. *Il1b* restricted the dissemination of bacteria by promoting bone marrow (BM) emergency granulopoiesis and, consistently, the induction of the neutrophil differentiation factor granulocyte colony-stimulating factor (G-CSF) upon infection. In contrast, *Il1a* was dispensable for the containment of bacteria and neutrophilia so that its essential role in protection against GAS infection was in line with enhancing host resistance. The distinct host protecting functions of *Il1a* and *Il1b* were reflected by markedly different effects of *Il1a* and *Il1b* on the tissue transcriptome: *Il1a* was the key driver of infection-induced transcriptional reprogramming of multiple metabolic pathways in the liver, whereas *Il1b* was required for the regulation of the spleen transcriptome. This distinct and organ-specific transcriptome regulation by *Il1a* and *Il1b* was not caused by tissue-dependent differences in responses to these cytokines; rather they correlated with different expression levels of each of the two cytokines in a given tissue. The differences between *Il1a* and *Il1b* during GAS infection were similar in a model of lung infection with *Streptococcus pneumoniae*, suggesting a broader relevance of our findings.

RESULTS

Il1a and *Il1b* are each required for host defense against GAS

In previous studies, we and others demonstrated the requirement for IL-1 receptor (*Il1r1*) signaling in defense of mice against invasive subcutaneous infection with GAS, i.e., a model of necrotizing fasciitis in humans (*12*, *24*). It remained open whether *Il1a* and *Il1b* were redundant in triggering the *Il1r1*-dependent protective response. Both *Il1a* and *Il1b* mRNAs were induced in the lesion, i.e., in the site of pathogen administration, 24 hours postinfection (p.i.), but *Il1b* induction was by two orders of magnitude higher than that of *Il1a* (17-fold versus 5641-fold, respectively) (fig. S1A). This implied that *Il1r1*-dependent host responses could be elicited by either of the two cytokines. To assess the requirement for *Il1a* or *Il1b* or both in host protection, we used $Il1a^{-/-}$ and $Il1b^{-/-}$ mice. First, we tested whether the absence of *Il1a* affected the expression of *Il1b* or vice versa. The expression levels of *Il1a* in the infection site were similar in $Il1b^{-/-}$ and WT mice 24 hours p.i. (fig. S1B). As expected, *Il1a* was not detected in $Il1a^{-/-}$ mice (fig. S1B). Similarly, *Il1b* expression was comparable in $Il1a^{-/-}$ and WT mice and was undetectable in $Il1b^{-/-}$ mice (fig. S1B). These results demonstrated that the absence of one of the two IL-1 cytokines did not lead to compensatory or impaired expression of the other one.

Survival experiments revealed that $Il1a^{-/-}$ and $Il1b^{-/-}$ mice were significantly more susceptible than WT mice ($P < 0.0001$), establishing that *Il1a* and *Il1b* are nonredundant and essential cytokines in defense against GAS infection (Fig. 1A). The susceptibility of $Il1a^{-/-}$ and $Il1b^{-/-}$ mice was comparable ($P > 0.05$). $Il1r1^{-/-}$ mice were more vulnerable than WT mice ($P < 0.001$) (Fig. 1A), as reported previously (*12*). $Il1r1^{-/-}$ mice were more susceptible than $Il1b^{-/-}$ mice ($P < 0.01$), indicating that a complete lack of IL-1 signaling was more detrimental than the deficiency in one of the two IL-1 receptor agonists (Fig. 1A). Tissue damage markers were not consistently different in the sera of $Il1a^{-/-}$, $Il1b^{-/-}$, or $Il1r1^{-/-}$ mice as compared to WT controls 24 hours p.i. The liver damage markers bilirubin and the aspartate transaminase–to–alanine transaminase (AST/ALT) ratio were not increased in $Il1a^{-/-}$, $Il1b^{-/-}$, and $Il1r1^{-/-}$, while glutamate dehydrogenase (GLDH) levels were elevated in $Il1r1^{-/-}$ and $Il1a^{-/-}$, but not $Il1b^{-/-}$, mice compared to WT controls (fig. S1C). The muscle damage marker creatinine was higher in $Il1r1^{-/-}$ mice, but creatine kinase was not increased (fig. S1C). Urea, the marker of prerenal failure, was increased in $Il1a^{-/-}$, but not in $Il1r1^{-/-}$ and $Il1b^{-/-}$, mice compared to WT mice (fig. S1C).

The assessment of the necrotic area at the site of infection revealed unexpected differences between $Il1a^{-/-}$ and $Il1b^{-/-}$ mice: The lesion size in $Il1a^{-/-}$ mice was comparable to that in WT mice, while $Il1b^{-/-}$ and $Il1r1^{-/-}$ exhibited larger necrotic areas (Fig. 1B). The largest lesion size was detected in $Il1r1^{-/-}$ mice consistent with the most severely impaired defense. Further differences between $Il1a^{-/-}$ and $Il1b^{-/-}$ mice were observed in tissue destruction in the lesion area: Tissue destruction was more pronounced in $Il1b^{-/-}$ and $Il1r1^{-/-}$ mice as compared to $Il1a^{-/-}$ and WT mice (Fig. 1, C and D, and fig. S1D). Moreover, Gram staining indicated that GAS was invading deeper tissues in $Il1b^{-/-}$ and $Il1r1^{-/-}$ mice as compared to WT controls. In contrast, the spreading of GAS in $Il1a^{-/-}$ mice was similar to that in WT mice (Fig. 1C). The invading bacteria were accompanied with $CD45^+$ and $Ly6G^+$ leukocytes but the colocalization of pathogens and immune cells was reduced in $Il1b^{-/-}$ and $Il1r1^{-/-}$ mice (Fig. 1, C and D).

In conclusion, *Il1a* and *Il1b* are each required for host defense against GAS infection. However, *Il1b*-deficient mice display more severe impact at the site of infection than *Il1a*-deficient and WT mice. These results imply different modes of action of *Il1a* and *Il1b* in response to GAS infection. Both of these modes appear to be required for maximum host protection since defense is most impaired in $Il1r1^{-/-}$ mice.

Il1b promotes bacterial clearance and enhances the neutrophilic barrier, while *Il1a* is dispensable for these processes

The deeper GAS invasion at the site of infection in $Il1b^{-/-}$ mice as compared to $Il1a^{-/-}$ and WT mice (Fig. 1, B and C) suggested that *Il1b*, not *Il1a*, was required for the local containment of bacteria. In agreement, $Il1b^{-/-}$ mice displayed a higher bacterial burden in distant tissues (liver, spleen, kidney, lung, and blood) 24 hours p.i. than $Il1a^{-/-}$ and WT mice (Fig. 2A). Bacterial loads were not different in $Il1a^{-/-}$ versus WT mice, indicating that GAS dissemination was not controlled by *Il1a* (Fig. 2A). $Il1r1^{-/-}$ mice displayed similar bacterial burdens as $Il1b^{-/-}$ mice in all organs except for the spleen in which they were slightly higher in $Il1r1^{-/-}$ mice (Fig. 2A). Since *Il1a* was not contributing to the containment of bacteria, the higher colony-forming units (CFU) in the spleen of in $Il1r1^{-/-}$ as compared to $Il1b^{-/-}$ mice were probably caused by the overall poorer defense of the *Il1r1*-deficient animals (Fig. 1A).

An important consequence of the GAS infection is hemolysis, which is caused by the activity of the cytolysins streptolysin O and streptolysin S (*25*). The higher bacterial counts in the blood of $Il1b^{-/-}$ mice suggested that hemolysis was likely to be more pronounced in these mice. In agreement, we detected increased hemolysis and heme levels in the blood of $Il1b^{-/-}$ mice as compared to $Il1a^{-/-}$ and WT mice (fig. S2, A and B).

The increased dissemination of GAS in the absence of *Il1b* indicated a defect in mechanisms critically important for the containment of

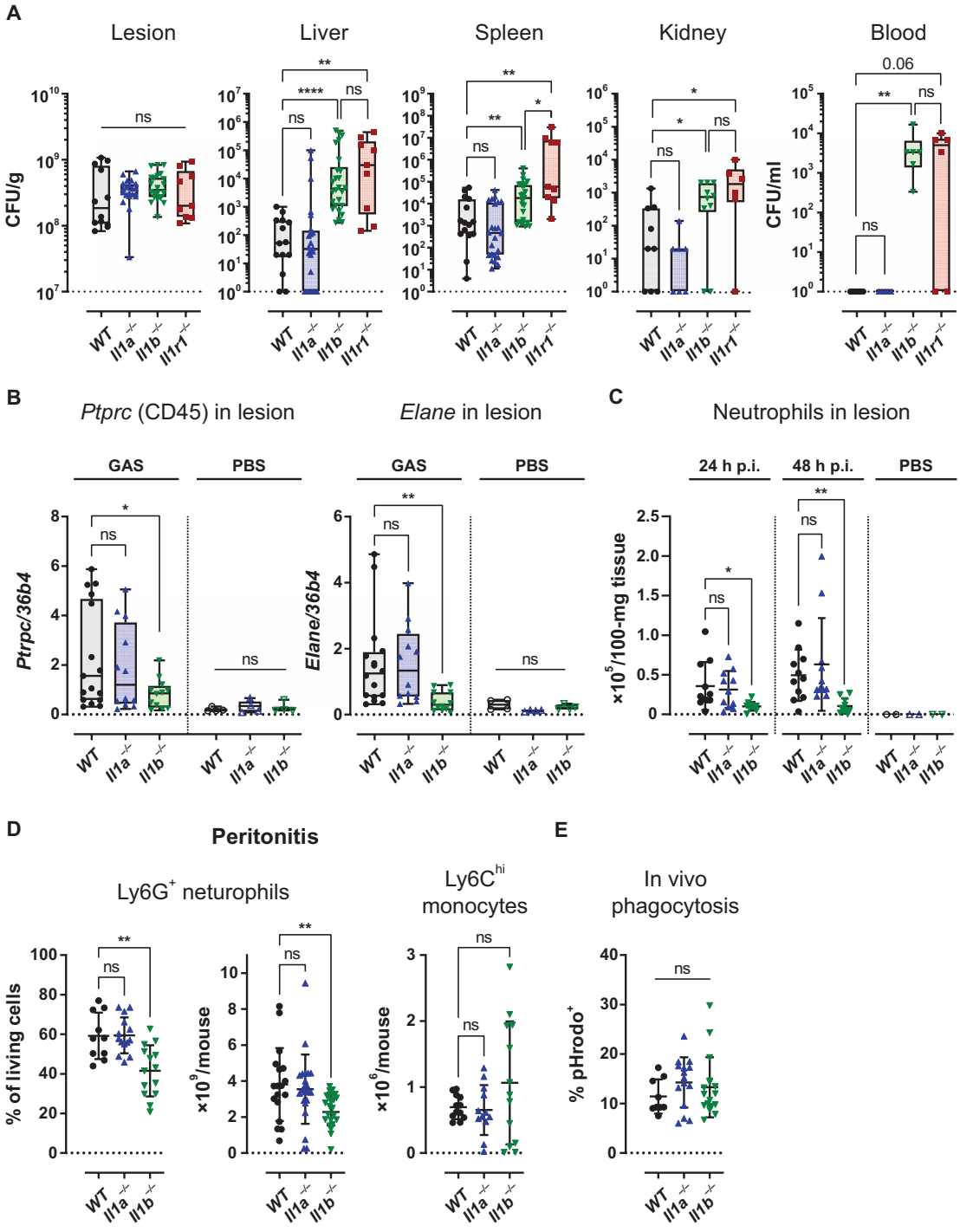

Fig. 2. Bacterial clearance and neutrophil infiltration are dependent on *Il1b* but not *Il1a*. (**A**) *Il1a*$^{-/-}$, *Il1b*$^{-/-}$, *Il1r1*$^{-/-}$, and WT mice were infected, and GAS loads in lesions, livers, spleens, kidneys, and blood were determined 24 hours p.i. as CFU per milliliter of blood or per gram of tissue per animal. For the lesion, liver, spleen, $n = 13$ (WT), $n = 24$ (*Il1a*$^{-/-}$), and $n = 24$ (*Il1b*$^{-/-}$). For the kidney, $n = 6$ to 9 per genotype; for the blood, $n = 5$ to 6 per genotype. Kruskal-Wallis with Dunn's multiple comparisons with median and 10th to 90th percentile. *$P < 0.05$; **$P < 0.01$; ****$P < 0.0001$. (**B**) *Ptprc* and *Elane* mRNA in lesions 24 hours p.i. (GAS) and in the skin and underlying muscular tissue from uninfected controls [phosphate-buffered saline (PBS)]. Box-and-whisker plot with median value and 10th to 90th percentile. Kruskal-Wallis with Dunn's multiple comparisons, $n = 6$ to 8 per genotype. *$P < 0.05$; **$P < 0.01$. (**C**) Neutrophil counts (CD45$^+$ CD11b$^+$ Ly6C^{med} Ly6G$^+$) in lesions 24 and 48 hours p.i. (GAS, $n = 11$ per genotype) and in the skin tissue from uninfected controls [phosphate-buffered saline (PBS), $n = 2$ per genotype]. Student's *t* test. *$P < 0.05$; **$P < 0.01$. (**D**) Neutrophil and monocyte recruitment in peritonitis induced by heat-killed (HK) GAS. Numbers of neutrophils (CD45$^+$ CD11b$^+$ Ly6C^{med} Ly6G$^+$) in percent of living cells (left) or per mouse (middle) and of monocytes (CD45$^+$ CD11b$^+$ Ly6G$^-$ Ly6C^{hi}) per mouse (right) were determined 24 hours after induction. Student's *t* test, $n = 8$ to 15 per genotype. **$P < 0.01$. (**E**) In vivo phagocytosis by peritoneal neutrophils. Mice were primed by injection of heat killed GAS, followed by injection of pHrodo-stained HK GAS 18 hours later. Numbers of pHrodo$^+$ neutrophils were normalized to total neutrophils numbers. One-way analysis of variance (ANOVA), $n = 9$ (WT), $n = 15$ (*Il1a*$^{-/-}$), and $n = 17$ (*Il1b*$^{-/-}$).

the pathogen. We decided to initially examine neutrophil accumulation as this leukocyte subset is an essential component of the barrier against GAS dissemination (*12*, *26*–*28*). The mRNA levels of the general leukocyte marker *Ptrpc* (encoding the CD45 protein) and the neutrophil elastase gene *Elane* at the site of infection were lower in *Il1b*$^{-/-}$ mice than in *Il1a*$^{-/-}$ and WT mice in the lesion 24 hours p.i. (Fig. 2B). In agreement, flow cytometry analysis of the lesion revealed lower numbers of infiltrating neutrophils (CD45^{+} CD11b^{+} Ly6C^{med} Ly6G^{+}) in *Il1b*$^{-/-}$ mice when compared to *Il1a*$^{-/-}$ and WT mice 24 and 48 hours p.i. (Fig. 2C and fig. S2C). Similar effects of *Il1b* deficiency were observed in a model of GAS-induced peritonitis: Neutrophils (total numbers as well as percentage in leukocytes) in the peritoneal cavity were lower in *Il1b*$^{-/-}$ mice when compared to *Il1a*$^{-/-}$ and WT mice (Fig. 2D and fig. S2D). In contrast, monocyte counts were similar in all genotypes (Fig. 2D and fig. S2D). Notably, phagocytosis, which is an important neutrophilic mechanism of GAS clearance (*26*), was not impaired in the absence of either *Il1a* or *Il1b* (Fig. 2E and fig. S2E).

In summary, these data demonstrate that *Il1b*, not *Il1a*, is vital for congregation of neutrophils at the infection site and pathogen clearance. Thus, *Il1b* drives resistance against GAS as it activates mechanisms targeting the pathogen. In contrast, the critical role of *Il1a* in host protection is consistent with an augmentation of tolerance rather than resistance.

Il1b promotes G-CSF production and emergency granulopoiesis

Il1r1 is known to be required for alum-induced emergency granulopoiesis (*29*). We thus asked whether a deficient GAS-induced emergency granulopoiesis is the cause of lower neutrophil numbers at the site of infection observed in *Il1b*$^{-/-}$ mice (Fig. 2C). Blood counts measured using a hematology analyzer revealed lower granulocyte numbers in *Il1b*$^{-/-}$ mice when compared to *Il1a*$^{-/-}$ and WT mice 24 hours p.i. (Fig. 3A). This difference was not seen in naïve [phosphate-buffered saline (PBS)–treated] mice (Fig. 3A). As expected, infected mice displayed higher granulocyte numbers when compared to naïve mice owing to infection-induced emergency granulopoiesis. The monocyte and lymphocyte populations were not affected by the lack of *Il1b* (Fig. 3A). The specific impact of *Il1b* deficiency on blood neutrophils was confirmed using flow cytometry (neutrophils, CD45^{+} CD11b^{+} Ly6C^{med} Ly6G^{+}; monocytes, CD45^{+} CD11b^{+} Ly6G^{-} Ly6C^{hi}; T cells, CD45^{+} CD3^{+}) (fig. S3A).

The lower numbers of blood neutrophils in infected *Il1b*$^{-/-}$ mice could be caused by a reduction in the BM neutrophil pool. However, BM neutrophils (CD45^{+} CD11b^{+} Ly6C^{med} Ly6G^{+}) were not decreased in *Il1b*$^{-/-}$ mice as compared to *Il1a*$^{-/-}$ and WT mice 24 hours p.i. (Fig. 3B and fig. S3B). The neutrophil counts were also similar in uninfected mice in all genotypes (Fig. 3B and fig. S3B). Predictably, BM neutrophil numbers were diminished during infection owing to neutrophil mobilization (Fig. 3B and fig. S3B), which coincided with neutrophilia in the blood (Fig. 3A). BM monocytes (CD45^{+} CD11b^{+} Ly6G^{-} Ly6C^{hi}) were comparable in all genotypes (Fig. 3B and fig. S3B). Together, the lower number of blood neutrophils in *Il1b*$^{-/-}$ mice 24 hours p.i. did not mirror changes in the BM compartment.

Mature neutrophils are known to rapidly egress from BM upon GAS infection (*30*). This inflammatory mobilization leads to low numbers of BM neutrophils. We hypothesized that the rapid mobilization of BM neutrophils upon infection might prevent robust detection of differences in neutrophil production. To directly address the generation of mature neutrophils during reactive granulopoiesis in BM, we analyzed progenitor cells developing from self-renewing pluripotent hematopoietic stem cells (HSCs). The numbers of Lin^{-} cells (CD5^{-} CD45R^{-} CD11b^{-} Gr-1^{-} 7-4^{-} Ter-119^{-}) and early lymphoid precursors (Lin^{-} Sca-1^{+} c-Kit^{hi}) (*31*)) were comparable in *Il1a*$^{-/-}$, *Il1b*$^{-/-}$, and WT mice both 24 hours p.i. and in PBS-treated controls (Fig. 3C). Similarly, the numbers of common myeloid progenitors (CMPs) (Lin^{-} Sca-1^{-} c-Kit^{hi} CD16/32^{lo} CD34^{+}) did not display differences between the genotypes (Fig. 3D and fig. S3, C and D). However, granulocyte-macrophage progenitors (GMPs) (Lin^{-} Sca-1^{-} c-Kit^{hi} CD16/32^{hi}, CD34^{lo}), which develop from CMPs (*31*), were reduced in *Il1b*$^{-/-}$ mice when compared to *Il1a*$^{-/-}$ and WT mice 24 hours p.i. (Fig. 3D and fig. S3D). Thus, GMPs, unlike other hematopoietic progenitors, were dependent on *Il1b*.

GMPs give rise to monocytes and granulocytes (including neutrophils) (*31*). We observed lower numbers of neutrophils but not monocytes in the blood of infected *Il1b*$^{-/-}$ mice (Fig. 3A). This phenotype resembled hematopoietic impediments observed in mice lacking the *Csf3* gene that codes for the G-CSF (*32*). *Csf3*$^{-/-}$ mice show lower numbers of GMPs and decreased neutrophil numbers particularly during emergency granulopoiesis (*32*). Monocytes are barely impaired in young *Csf3*$^{-/-}$ mice (*32*). The hematopoietic similarities between *Csf3*$^{-/-}$ and *Il1b*$^{-/-}$ mice prompted us to assess *Csf3* mRNA expression and G-CSF protein levels in our system. The analysis revealed that the serum G-CSF was lower in *Il1b*$^{-/-}$ mice as compared to *Il1a*$^{-/-}$ and WT mice 24 hours p.i. (Fig. 3E). Infection did not increase *Csf3* expression in BM, suggesting that this tissue was not the source of the infection-induced serum G-CSF (fig. S3E). In contrast, *Csf3* mRNA was induced in the site of infection 24 hours p.i., and the induction was markedly lower in *Il1b*$^{-/-}$ mice as compared to *Il1a*$^{-/-}$ and WT mice (Fig. 3F). These results indicated that *Il1b* is a critical activator of *Csf3* expression in the lesion. The requirement for *Il1b*, not *Il1a*, in the induction of *Csf3* mRNA is in line with high *Il1b* and low *Il1a* expression in the lesion (Fig. 1B). Since muscle cells are functional producers of G-CSF (*33*, *34*), the *Il1b*-induced serum G-CSF is likely to originate from muscle tissue that is associated with the lesion samples (Fig. 1C).

In summary, the results describe a specific requirement for *Il1b* in *Csf3* induction in the lesion and in emergency granulopoieses during infection with GAS. The findings suggest that the high susceptibility of *Il1b*$^{-/-}$ mice to GAS infection is caused by deficient emergency granulopoieses, which results from impaired *Csf3* induction.

Il1a and *Il1b* deficiencies affect tissue transcriptomes in distinct ways during GAS infection

The finding that GAS-induced C*sf3* expression is largely dependent on *Il1b* and not on *Il1a* (Fig. 3E) indicated that these cytokines have distinct impacts on gene expression. To investigate the effects of *Il1a* and *Il1b* on gene expression in detail, we analyzed the spleen and liver transcriptomes of *Il1a*$^{-/-}$, *Il1b*$^{-/-}$, and WT mice 24 hours p.i. using RNA sequencing (RNA-seq). These organs harbor cells known to require IL-1R signaling for physiological responses: Hepatocyte-specific *Il1r1* deletion ameliorates acute liver injury (*35*), and dendritic cells found, among other tissues, in the spleen need *Il1r1* for mounting adaptive immunity against influenza virus (*36*).

Principal components analysis (PCA) of liver and spleen RNA-seq derived from infected *Il1a*$^{-/-}$, *Il1b*$^{-/-}$, and WT mice showed high

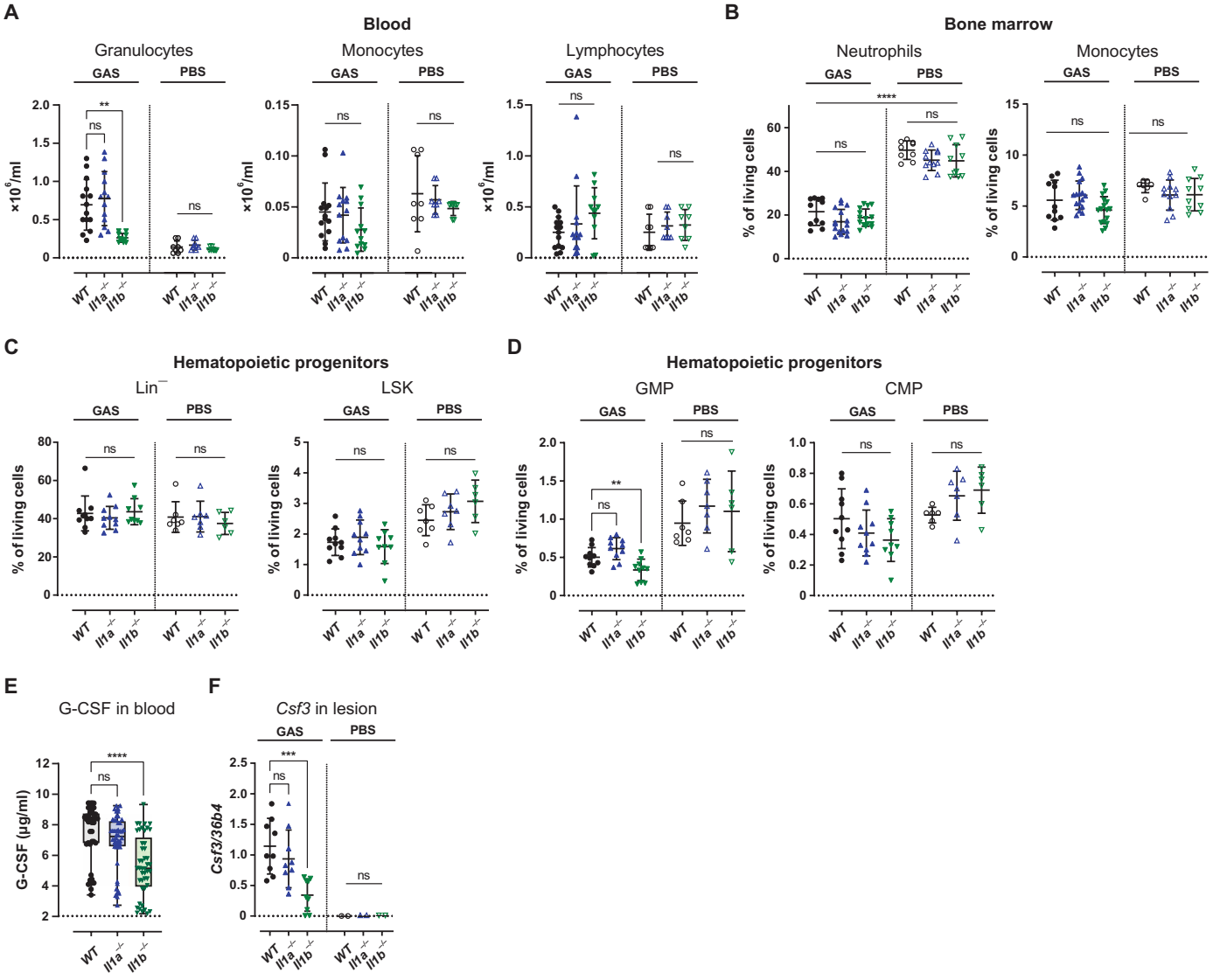

Fig. 3. *Il1b* is driver of emergency hematopoiesis. (**A**) Granulocyte, monocyte, and lymphocyte numbers in the blood of *Il1a*$^{-/-}$, *Il1b*$^{-/-}$, and WT mice 24 hours p.i. (GAS) and in uninfected controls (PBS), as determined using a hematology analyzer. ANOVA with Dunnett's correction for multiple comparisons, $n = 8$ to 14 per genotype. $^{**}P < 0.01$. (**B**) Neutrophil (CD45$^+$ CD11b$^+$ Ly6C^{med} Ly6G$^+$) and monocyte (CD45$^+$ CD11b$^+$ Ly6G$^-$ Ly6C^{hi}) percentages (of living cells) in BM from *Il1a*$^{-/-}$, *Il1b*$^{-/-}$, and WT mice 24 hours p.i. (GAS) and from uninfected controls (PBS), as determined flow cytometry. One-way ANOVA, 10 to 16 per genotype. $^{****}P < 0.0001$. (**C**) Lin$^-$ progenitor cells (CD5$^-$ CD45R$^-$ CD11b$^-$ Gr-1$^-$ 7-4$^-$ Ter-119$^-$) and early lymphoid precursors (LSK) (Lin$^-$ Sca-1$^+$ c-Kit^{hi}) in BM from *Il1a*$^{-/-}$, *Il1b*$^{-/-}$, and WT mice 24 hours p.i. (GAS) and from uninfected mice (PBS), as determined by flow cytometry. ANOVA with Dunnett's correction for multiple comparisons, $n = 7$ to 10 per genotype. (**D**) Common myeloid progenitors (CMPs) (Lin$^-$ Sca-1$^-$ c-Kit^{hi} CD16/32^{lo}, CD34$^+$) and granulocyte-macrophage progenitors (GMPs) (Lin$^-$ Sca-1$^-$ c-Kit^{hi} CD16/32^{hi}, CD34^{lo}) in BM from *Il1a*$^{-/-}$, *Il1b*$^{-/-}$, and WT mice 24 hours p.i. (GAS) and from uninfected controls (PBS), as determined by flow cytometry. ANOVA with Dunnett's correction for multiple comparisons, $n = 7$ to 10 per genotype. $^{**}P < 0.01$. (**E** and **F**) G-CSF protein (encoded by the *Csf3* gene) (E) and *Csf3* mRNA levels (F) at the site of infection from *Il1a*$^{-/-}$, *Il1b*$^{-/-}$, and WT mice 24 hours p.i. (GAS) and (for *Csf3* mRNA) from uninfected controls (PBS), as determined by enzyme-linked immunosorbent assay (ELISA) and reverse transcription quantitative polymerase chain reaction (RT-qPCR), respectively. Kruskal-Wallis with Dunn's multiple comparisons (E), $n = 22$ to 24 per genotype. $^{***}P < 0.001$; $^{****}P < 0.0001$.

intrareplicate reproducibility and sample clustering according to the genotype in each organ (Fig. 4A and data S1 and S2). The analysis indicated that *Il1a* and *Il1b* have different effects on the transcriptome in both the liver and the spleen. Clusters of *Il1b*$^{-/-}$ and WT replicates were closer to each other than to the *Il1a*$^{-/-}$ cluster in the liver. In contrast, the *Il1b*$^{-/-}$ replicates formed a cluster that was separated from the *Il1a*$^{-/-}$ and WT clusters in the spleen (Fig. 4A). This suggested that *Il1a* was more important for the liver transcriptome, whereas *Il1b* was played a major in the spleen transcriptome during infection. The distinct effects of *Il1a* and *Il1b* deficiencies were confirmed by differential expression analysis (Fig. 4B and data S3). *Il1a*$^{-/-}$ and WT (*Il1a*$^{-/-}$_inf versus WT_inf) liver transcriptomes differed in the expression of 281 genes [adjusted *P* value (*P*adj) < 0.001, $|\log_2$ fold change| (lfc) > 1], whereas the difference between *Il1b*$^{-/-}$ and WT samples (*Il1b*$^{-/-}$_inf versus WT_inf) comprised only 53 differently expressed genes (Fig. 4B and data S3). In contrast, *Il1a* deletion had only a minor impact in the spleen (20 differently expressed genes in *Il1a*$^{-/-}$_inf versus WT_inf comparison), while *Il1b* deletion resulted

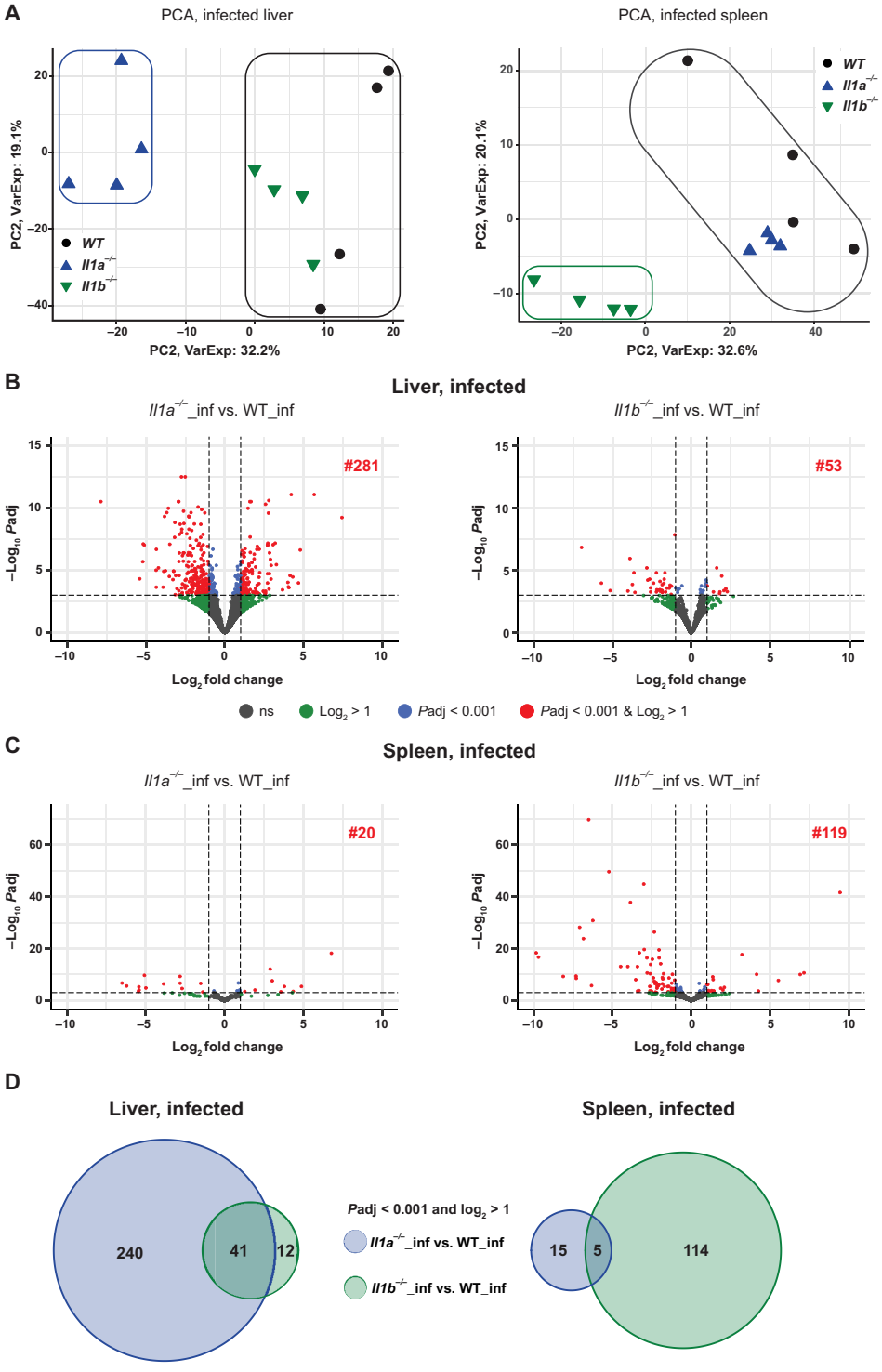

Fig. 4. *Il1a* deficiency during infection strongly affects the liver transcriptome, whereas *Il1b* deficiency results in major changes in the spleen transcriptome. (**A**) PCA plots of liver and spleen RNA-seq derived from *Il1a*$^{-/-}$, *Il1b*$^{-/-}$, and WT mice 24 hours p.i. *Il1a*$^{-/-}$ replicates (blue ellipse) are separated from WT and *Il1b*$^{-/-}$ replicates (black ellipse) in the liver (left). *Il1b*$^{-/-}$ replicates (green ellipse) are separated from WT and *Il1a*$^{-/-}$ replicates (black ellipse) in the spleen (right). (**B** and **C**) Differential expression analysis of liver (B) and spleen (C) RNA-seq from infected *Il1a*$^{-/-}$ versus infected WT mice (*Il1a*$^{-/-}$_inf versus WT_inf) (left) and infected *Il1b*$^{-/-}$ versus infected WT mice (*Il1b*$^{-/-}$_inf versus WT_inf) (right). Genes with differential expression values *P*adj < 0.001 and lfc > 1 are highlighted in red, and their number is indicated within the volcano plots. (**D**) Visualization of genes regulated by both *Il1a* and *Il1b* in the liver (left, Venn diagram) and the spleen (right, Venn diagram). Genes regulated by *Il1a* (*P*adj < 0.001, lfc > 1) were identified in differential expression analyses shown in (B) and (C) in the comparison *Il1a*$^{-/-}$_inf versus WT_inf, while genes regulated by *Il1b* were identified in the comparison *Il1b*$^{-/-}$_inf versus WT_inf. The number of genes regulated by both *Il1a* and *Il1b* is displayed in the overlaps.

in robust gene expression changes (119 differently expressed in *Il1b*$^{-/-}$_inf versus WT_inf comparison) (Fig. 4C and data S2). The regulation of *Csf3* by *Il1b*, as shown in lesion (Fig. 3F), could not be assessed in the liver and spleen because of low expression: *Csf3* counts were below the detection limit in the liver and low in the spleen (mean normalized counts = 2) from infected WT mice (data S1 and S2). Hence, these organs were not relevant sources of G-CSF.

Visualization of genes regulated by both *Il1a* and *Il1b* in the liver (*P*adj <0.001, lfc > 1) revealed that *Il1a*-dependent genes comprised most of the *Il1b*-dependent genes (41 of 53 genes) (Fig. 4D). Thus, *Il1a* and *Il1b* regulated a different number but not a different spectrum of genes in the liver. Similarly, the overlap of *Il1a*-dependent versus *Il1b*-dependent genes in the spleen comprised five genes, which is a substantial proportion of *Il1a*-dependent genes in this organ (Fig. 4D). In contrast, the spectrum of genes regulated by either of the two cytokines in both the liver and the spleen was different, consistent with diverse gene expression profiles in these organs (e.g., one gene was regulated by *Il1a* in both the liver and spleen) (fig. S4).

Together, two important conclusions can be drawn from the transcriptome analysis in infected mice. First, *Il1a* and *Il1b* deficiencies result in distinct impacts on the transcriptome in a given tissue, as evident from liver and spleen analyses. Second, the effects of *Il1a* and *Il1b* deficiencies differ in different tissues: The liver transcriptome is largely *Il1a* dependent, while the spleen transcriptome is more strongly regulated by *Il1b* during infection.

Il1a is driver of liver transcriptome reprogramming in response to infection

The stark difference between the liver transcriptomes from *Il1a*$^{-/-}$ versus WT mice 24 hours p.i. (Fig. 4, A and B) prompted us to investigate whether *Il1a* regulates the liver gene expression in response to infection or already in naïve mice. To this end, we analyzed the liver transcriptomes of uninfected PBS-treated *Il1a*$^{-/-}$, *Il1b*$^{-/-}$, and WT mice with the aim to compare them to those of infected mice. PCA of samples from uninfected mice confirmed good reproducibility of replicates (Fig. 5A and data S1). Moreover, all uninfected samples clustered close to each other indicating similar variance of both principal components regardless of the genotype. PCA revealed a strong effect of infection on the liver transcriptome: All samples from infected mice were well separated from the uninfected samples (Fig. 5A). The analysis confirmed the more important role of *Il1a* as compared to *Il1b* in regulation of the liver transcriptome in infected mice (Fig. 4A). Differential expression analysis did not reveal significant differences between *Il1a*$^{-/-}$ versus WT livers before infection (*Il1a*$^{-/-}$_PBS versus WT_PBS) and only a few differences between *Il1b*$^{-/-}$ versus WT livers (*Il1b*$^{-/-}$_PBS versus WT_PBS) (Fig. 5B, fig. S5A, and data S4). This indicated the effect *Il1a* deficiency on the transcriptome observed in infected livers (Fig. 4) developed upon infection.

Comparison of liver samples from infected versus uninfected WT mice (WT_inf versus WT_PBS) confirmed that infection resulted in a deep reprogramming of the liver transcriptome (Fig. 5C and data S5). Comparisons of samples from infected versus uninfected *Il1a*$^{-/-}$ mice (*Il1a*$^{-/-}$_inf versus *Il1a*$^{-/-}$_PBS) showed that infection remodeled the liver transcriptome also in the absence of *Il1a* (Fig. 5C and data S5). Similarly, infection-induced transcriptome changes occurred also in the absence of *Il1b* (*Il1b*$^{-/-}$_inf versus *Il1b*$^{-/-}$_PBS) (fig. S5B and data S5). Moreover, comparison of *Il1a*$^{-/-}$ samples from infected mice to WT samples from uninfected mice (*Il1a*$^{-/-}$_inf versus WT_PBS) showed that the infection-associated transcriptome in *Il1a*$^{-/-}$ mice was different from the uninfected WT transcriptome (Fig. 5C and data S5). These results showed that the liver transcriptome is regulated during infection by IL-1 signaling–dependent and, as expected, IL-1 signaling–independent cues.

Overlap analysis between *Il1a*$^{-/-}$_inf versus *Il1a*$^{-/-}$_PBS and *Il1a*$^{-/-}$_inf versus WT_PBS comparisons revealed that most of the differentially expressed genes (*P*adj < 0.001, lfc > 1) in these comparisons were the same (Fig. 5D). Likewise, the effects of *Il1a* across all expressed genes in *Il1a*$^{-/-}$_inf versus *Il1a*$^{-/-}$_PBS comparison correlated with those in the *Il1a*$^{-/-}$_inf versus WT_PBS comparison ($R^2 = 0.98$; $y = -0.022 + x$) (fig. S5C). These analyses confirmed that the liver transcriptome in infected *Il1a*$^{-/-}$ mice was defined by the absence of *Il1a*-dependent infection–regulated genes. In conclusion, *Il1a* does not substantially regulate the liver transcriptome under steady-state conditions but is an important driver of transcriptome reprogramming in response to infection.

Adaptation of liver metabolic programs to infection is dependent on *Il1a*

The identification of infection-induced *Il1a*-dependent changes in the liver transcriptome (Figs. 4, A and B, and 5D) enabled us to analyze the impact of *Il1a* on specific liver responses during host defense. We performed gene set enrichment analysis (GSEA) for genes differentially expressed in *Il1a*$^{-/-}$ versus WT mice 24 hours p.i. (*Il1a*$^{-/-}$_inf versus WT_inf; lfc > 1, *P*adj <0.05; 281 genes) (data S1) using terms defined in the Gene Ontology (GO) database (http://geneontology.org/). The enrichment data (data S6) were visualized using the EnrichmentMap plug-in for Cytoscape (Fig. 6A). Similar GO terms (represented by nodes) were clustered, and related clusters were grouped to multiclusters (data S6). Four multiclusters were identified: Apoptosis & Vesicle signaling, Signaling, Metabolism, and Immune regulation (Fig. 6A). The multiclusters Apoptosis & Vesicle signaling and Signaling comprised GO terms that were positively enriched in the *Il1a*$^{-/-}$ data when compared to the WT dataset. The multiclusters Metabolism and Immune regulation represented GO terms that were negatively enriched in the *Il1a*$^{-/-}$ data relative to the WT dataset.

The largest number of nodes for GO terms was found in the negatively enriched multicluster Metabolism (42 nodes) (Fig. 6A and data S6). Moreover, the multicluster Metabolism was well defined as it consisted exclusively of clusters and GO terms representing metabolic pathways. This analysis showed that the induction of metabolic genes by infection was broadly impaired in the *Il1a*-deficient liver. Metabolic adjustments have been identified in several studies to protect the host by promoting tolerance to infection cues: pathways implicated in tolerance include triglyceride, amino acid, and carbohydrate metabolism (*37*–*39*). These pathways were found to be negatively enriched in the liver from infected *Il1a*$^{-/-}$ mice, suggesting a defective tolerance (Fig. 6A and data S6).

The multiclusters Apoptosis & Vesicle signaling, Signaling, and Immune regulation were characterized by the presence of various signaling clusters. The negatively enriched multicluster Immune regulation included a large cluster Immune cell regulation and proliferation implying a defect in induction of immune cell proliferation–associated genes in the absence of *Il1a* (Fig. 6A). The enriched multicluster Apoptosis & Vesicle signaling was dominated by the cluster Apoptotic signaling indicating uncontrolled induction of apoptosis-promoting

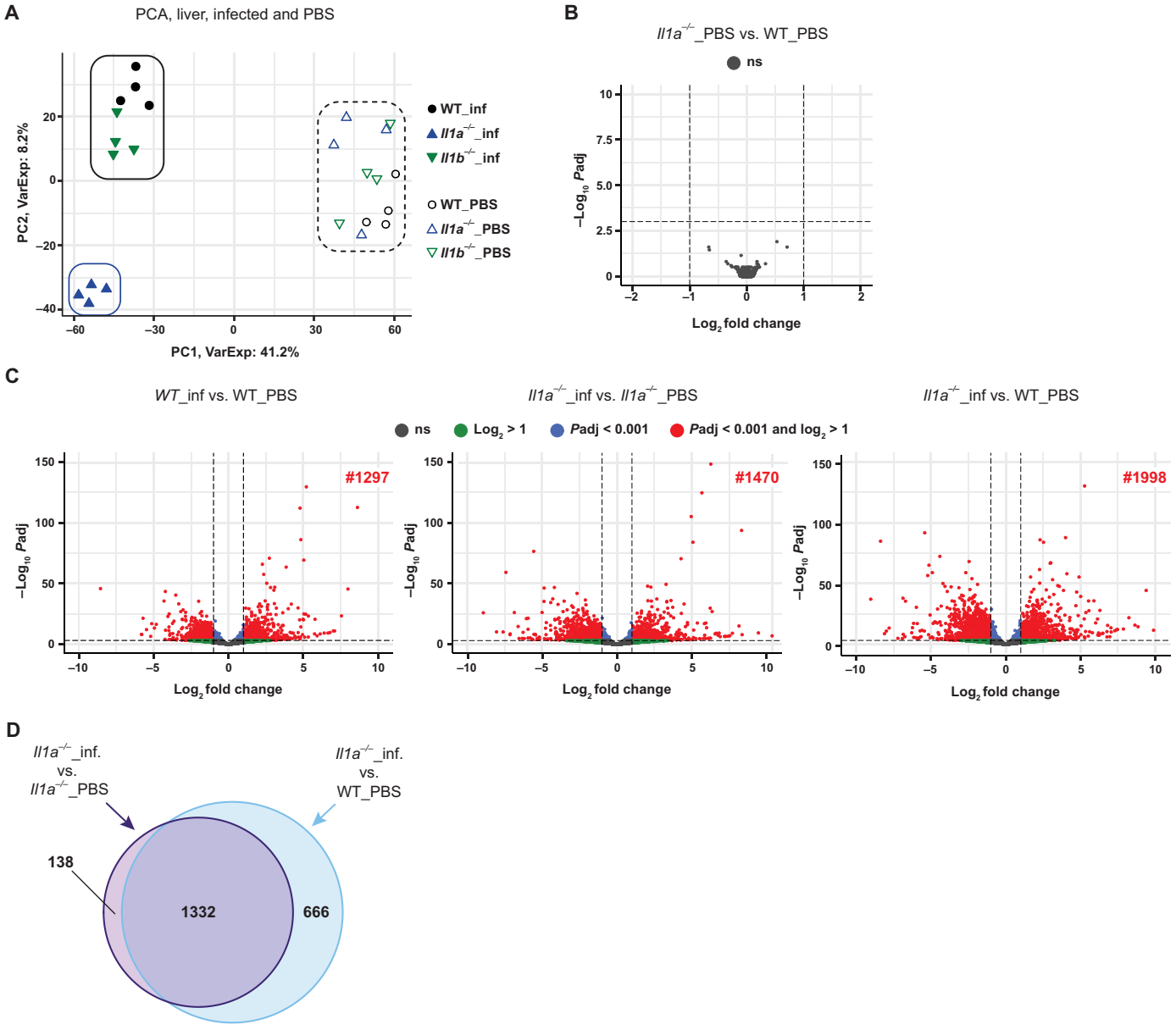

Fig. 5. *Il1a* is critical for infection-induced reprogramming of the liver transcriptome. (**A**) PCA plot of liver RNA-seq derived from *Il1a*$^{-/-}$, *Il1b*$^{-/-}$, and WT mice 24 hours p.i. and from uninfected mice (PBS). Replicates of all uninfected genotypes clustered together (dashed line ellipse) and were well separated from replicates of infected mice that formed a cluster comprising *Il1a*$^{-/-}$ samples (blue ellipse) and a cluster with samples from *Il1b*$^{-/-}$ and WT mice (black ellipse). (**B**) Differential expression analysis of liver RNA-seq from uninfected *Il1a*$^{-/-}$ versus uninfected WT mice (*Il1a*$^{-/-}$_PBS versus WT_PBS). No differentially expressed genes (*P*adj < 0.001 and lfc > 1) were detected. (**C**) Differential expression analysis of liver RNA-seq from infected versus uninfected WT mice (WT_inf versus WT_PBS) (left), infected versus uninfected *Il1a*$^{-/-}$ mice (*Il1a*$^{-/-}$_inf versus *Il1a*$^{-/-}$_PBS) (middle), and infected *Il1a*$^{-/-}$ mice versus uninfected WT mice (*Il1a*$^{-/-}$_inf versus WT_PBS) (right). Genes with differential expression values *P*adj <0.001 and lfc > 1 are highlighted in red and their number is indicated within the volcano plots. (**D**) Overlap analysis visualizing liver genes affected in infected *Il1a*$^{-/-}$ mice in comparison to uninfected *Il1a*$^{-/-}$ mice (*Il1a*$^{-/-}$_inf versus *Il1a*$^{-/-}$_PBS) or in comparison to uninfected WT mice (*Il1a*$^{-/-}$_inf versus WT_PBS). Note that most of the differentially regulated genes (*P*adj <0.001, lfc > 1) were in the overlap, confirming the high similarity of liver transcriptomes in uninfected *Il1a*$^{-/-}$ and WT mice.

genes in the *Il1a*-deficient liver transcriptome during infection. The enriched multicluster Signaling comprised clusters related to innate immune pathways such as Toll-like receptor (TLR) and chemokine signaling, suggesting unrestricted activation of genes involved in innate immune responses within *Il1a*$^{-/-}$ livers.

To display dysregulation of individual genes associated with each of the four multiclusters (Apoptosis & Vesicle signaling, Signaling, Metabolism, and Immune regulation), we used heatmaps using the same gene subset as for GSEA. These genes were assigned a ranking *z* score in the comparisons *Il1a*$^{-/-}$_inf versus WT_PBS, *Il1b*$^{-/-}$_inf versus WT_PBS and WT_inf versus WT_PBS to visualize differences in infection-mediated regulation between the genotypes. The comparison of each of the infected genotype (*Il1a*$^{-/-}$, *Il1b*$^{-/-}$, and WT) to uninfected WT (WT_PBS) was used since the liver transcriptomes from uninfected mice were comparable in all genotypes (Fig. 5B and fig. S5A). The heatmaps highlighted the marked difference of

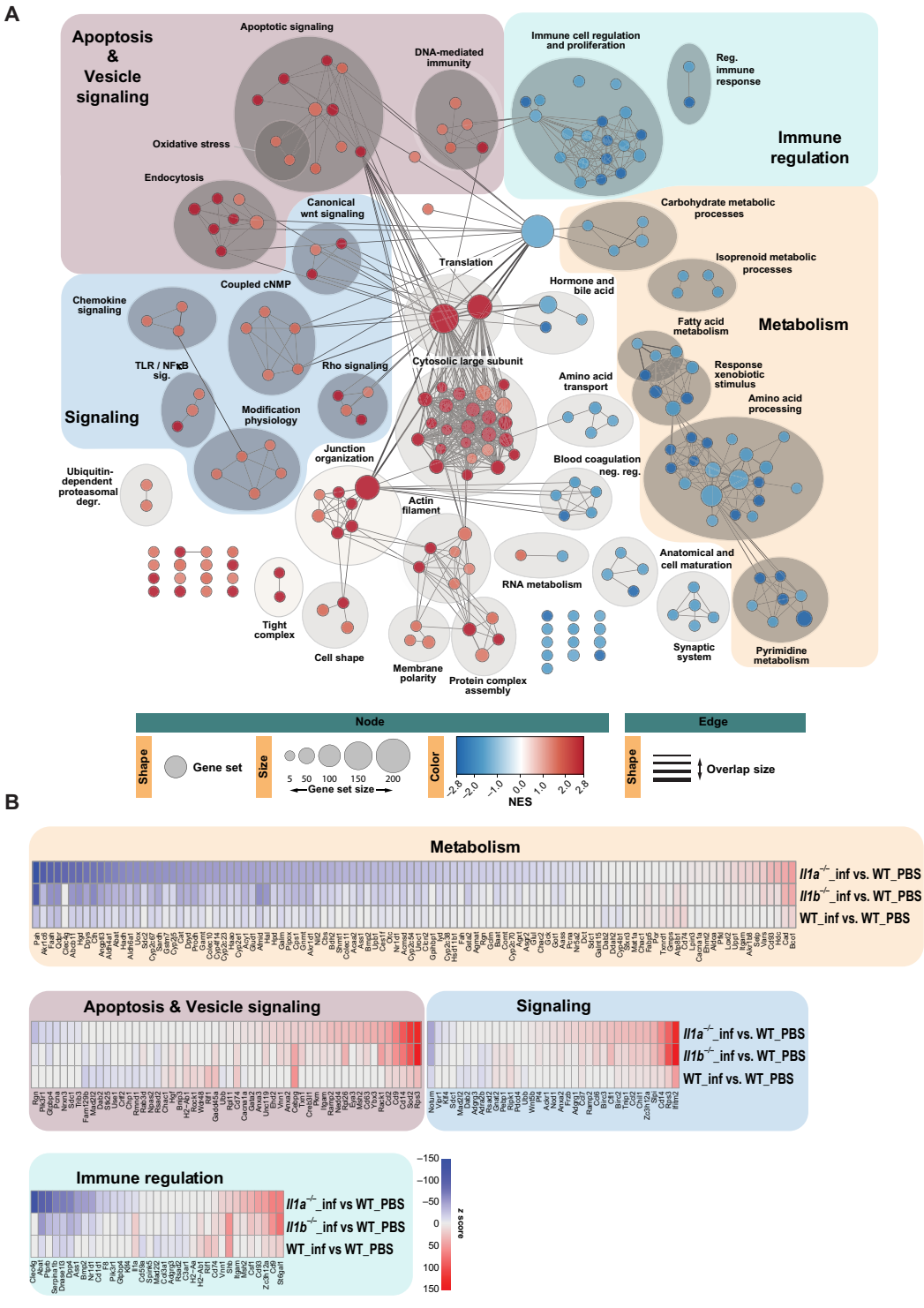

Fig. 6. Adjustments in liver metabolic pathways associated with host defense are dependent on *Il1a*. (**A**) Cytoscape map of GO terms enriched in a gene set comprising 281 genes differentially expressed in *Il1a*$^{-/-}$ versus WT livers (*Il1a*$^{-/-}$_inf versus WT_inf; lfc > 1, *P*adj <0.05) 24 hours p.i. Similar GO terms (represented by nodes) were grouped into clusters, and related clusters were merged into four multiclusters (Metabolism, Immune Regulation, Apoptosis & Vesicle signaling, and Signaling). Normalized enrichment score (NES) indicates negatively (blue) and positively (red) enriched GO terms in the *Il1a*$^{-/-}$ versus WT comparison. Note that the negatively enriched multicluster Metabolism contained the largest number of GO terms (*42*). cNMP, cyclic nucleotide. (**B**) Heatmaps visualizing infection-induced changes within the multiclusters defined in (A). The heatmaps highlight differences between infection-induced changes in *Il1a*$^{-/-}$ mice (*Il1a*$^{-/-}$_inf versus WT_PBS) from those in *Il1b*$^{-/-}$ mice (*Il1b*$^{-/-}$_inf versus WT_PBS) and WT mice (WT_inf versus WT_PBS) in all multiclusters.

Il1a-dependent infection–induced gene expression changes ($Il1a^{-/-}$_inf versus WT_PBS) from *Il1b*-dependent changes ($Il1b^{-/-}$_inf versus WT_PBS) and from changes in WT livers (WT_inf versus WT_PBS) (Fig. 6B). Moreover, the heatmaps showed that *Il1b*-dependent changes ($Il1b^{-/-}$_inf versus WT_PBS) resembled more the ones in WT livers (WT_inf versus WT_PBS) than changes that were *Il1a* dependent ($Il1a^{-/-}$_inf versus WT_PBS) (Fig. 6B). As expected, heatmaps showed that the gene set used for GO enrichment analysis in infected mice ($Il1a^{-/-}$_inf versus WT_inf) was not regulated by *Il1a* and *Il1b* in uninfected mice ($Il1a^{-/-}$_PBS versus WT_PBS; $Il1b^{-/-}$_PBS versus WT_PBS) (fig. S6).

These analyses demonstrated that *Il1a* drives adjustments in liver pathways associated with host defense. Depending on the pathway, *Il1a* can elicit inhibitory or stimulatory effects. *Il1a* is particularly critical for the induction of metabolic pathways known to be involved in tolerance to infection (*37*–*39*).

Distinct effects of *Il1a* versus *Il1b* in organs are determined by different local expressions of these cytokines during infection

IL-1α and IL-1β are considered to elicit the same signaling pathways and cellular responses (*1*, *2*). To verify this in our system and to exclude that differences in signaling cause cells from different tissues to activate distinct transcription programs, we investigated responses in relevant primary cells. We used primary hepatocytes as a major cell type present in the liver and BM-derived macrophages (BMDMs), which we considered as a representative of macrophages in the spleen. BMDMs from WT mice were treated with IL-1α or IL-1β, followed by the analysis of signaling events and gene expression changes. IL-1α and IL-1β caused comparable phosphorylation of inhibitor of NF-κB (IκB) and the MAP kinases p38 and extracellular signal–regulated kinase (ERK) (Fig. 7A; replicate in fig. S7A). Similar results were obtained when analyzing responses of hepatocytes to IL-1α and IL-1β (fig. S7B). Moreover, induction of *Tnf*, *Cxcl1*, *Il6*, *Ccl2*, and *Ccl3* in BMDMs and hepatocytes was similar in response to IL-1α and IL-1β (Fig. 7B and fig. S7C). These results confirmed that IL-1α and IL-1β trigger indistinguishable responses in target cells. Together, the data implied that the distinct impacts of *Il1a* and *Il1b* deficiencies on the liver and spleen transcriptomes during infection (Fig. 4) did not result from different responses to IL-1α and IL-1β by major cell types in these organs.

Thus, we considered the option that the differences between $Il1a^{-/-}$ and $Il1b^{-/-}$ transcriptomes in infected mice were caused by an unequal availability of IL-1α and IL-1β in the organ. This model is consistent with the observation that the differences between $Il1a^{-/-}$ and $Il1b^{-/-}$ transcriptomes during infection were high with regard to the number but not the identity of the affected genes (Fig. 4D). We then assessed the RNA-seq data (data S1) for *Il1a* and *Il1b* expression in the liver and spleen. The counts for each of these two genes in the corresponding knockout samples served as a reference baseline. The analysis revealed that *Il1a* was more strongly expressed in the liver from infected WT mice than *Il1b*: The mean of normalized *Il1a* counts were fivefold higher than the *Il1b* counts (131.4 versus 26.7 counts) (Fig. 7C). The analysis of the spleen dataset unraveled an opposite pattern of *Il1a* and *Il1b* expression: The *Il1b* counts were 18-fold higher than the *Il1a* counts (298.3 versus 16.6 counts) in WT samples (Fig. 7C). Notably, the expression of *Il1a* was not impaired in $Il1b^{-/-}$ samples and vice versa (Fig. 7C). Analysis of cytokine levels in tissues 24 hours p.i. using enzyme-linked immunosorbent assay (ELISA) showed that IL-1α and IL-1β bioavailability reflected the *Il1a* and *Il1b* mRNA levels: IL-1α levels were high in the liver but low in the spleen, while IL-1β showed the opposite pattern (Fig. 7, D and E). The lesion contained high levels of IL-1β and low amounts of IL-1α (Fig. 7, D and E), which correlated with *Il1a* and *Il1b* mRNA expression (fig. S1B). These experiments confirmed that the production of either of the two cytokines was not affected by the lack of the other one: IL-1α levels were similar in WT and $Il1b^{-/-}$ mice, and IL-1β levels were comparable in WT and $Il1a^{-/-}$ mice (Fig. 7, D and E). The regular production of IL-1α in $Il1b^{-/-}$ mice and of IL-1β in $Il1a^{-/-}$ mice persisted at least 48 hours (i.e., until close to death of the knockout mice), indicating that IL-1α and IL-1β were produced independently of each other throughout the infection (fig. S7D). Consistently, maturation of IL-1β proceeded normally in the absence of IL-1α as probed by Western blot analysis of the lesion 24 and 48 hours p.i. (Fig. 7F and fig. S7E). The production of IL-1α and IL-1β was further validated by the analysis of peritoneal macrophages from in $Il1a^{-/-}$, $Il1b^{-/-}$, and WT mice: LPS stimulation combined with nigericin treatment resulted in comparable levels of IL-1α in the cell supernatants of $Il1b^{-/-}$ and WT cells and, conversely, IL-1β levels were not affected by *Il1a* deficiency (fig. S7F). As expected, tumor necrosis factor (Tnf) secretion was similar in all genotypes. Similar results were obtained when using BMDMs (fig. S7G). These data also showed that IL-1α production was not impaired by *Il1b* deficiency in our system, in contrast to previously reported reduction in IL-1α production by *Il1b*-deficient BMDMs in context of fatty acid or adenosine 5′-triphosphate stimulation (*40*).

Pores formed by activated gasdermin D (GSDMD) are critical for execution of pyroptosis and release of IL-1β (*41*, *42*). The Western blotting analysis also demonstrated the activation of GSDMD upon GAS infection (Fig. 7F and fig. S7E). To examine whether GSDMD contributes to defense against GAS infection, we analyzed $Gsdmd^{-/-}$ mice. $Gsdmd^{-/-}$ mice were more vulnerable to infection than WT animals, and their susceptibility was similar as that of $Il1b^{-/-}$ mice (Fig. 7G). Bacterial loads were increased in the spleen of $Gsdmd^{-/-}$ mice as compared to WT controls 24 hours p.i. (fig. S7H). $Il1b^{-/-}$ mice exhibited higher bacterial loads in all analyzed tissues (fig. S7H), consistent with the experiment shown in Fig. 2A. The counts of blood granulocytes were lower in $Gsdmd^{-/-}$ mice when compared to WT controls, and the reduction of granulocyte numbers was similar to that in $Il1b^{-/-}$ mice (Fig. 7G). These data reveal a requirement for GSDMD in host defense against GAS. Moreover, the defect in blood granulocyte numbers and the higher bacterial counts in the spleen indicate a role of GSDMD in resistance, similar to the function of *Il1b*. However, the phenotype of $Gsdmd^{-/-}$ mice during GAS infection was less severe than that of $Il1b^{-/-}$ mice since the bacterial loads were increased in the spleen but not in other tissues and the defect in reactive granulopoiesis was less pronounced.

Cumulatively, the data established distinct expression patterns of *Il1a* versus *Il1b* in organs of infected mice. *Il1a* mRNA and protein levels were higher than those of *Il1b* in the liver that was consistent with the stronger impact of *Il1a* deficiency on the liver transcriptome 24 hours p.i. (Fig. 4). In further support of this, a detailed time course analysis in the liver revealed that the expression of *Il1a* was more strongly induced during infection than that of *Il1b* throughout the infection (Fig. 7H). Thus, the distinct effects of *Il1a* and *Il1b* deficiencies on the transcriptome in a given organ are not likely to be caused by different responses of tissues to IL-1α and

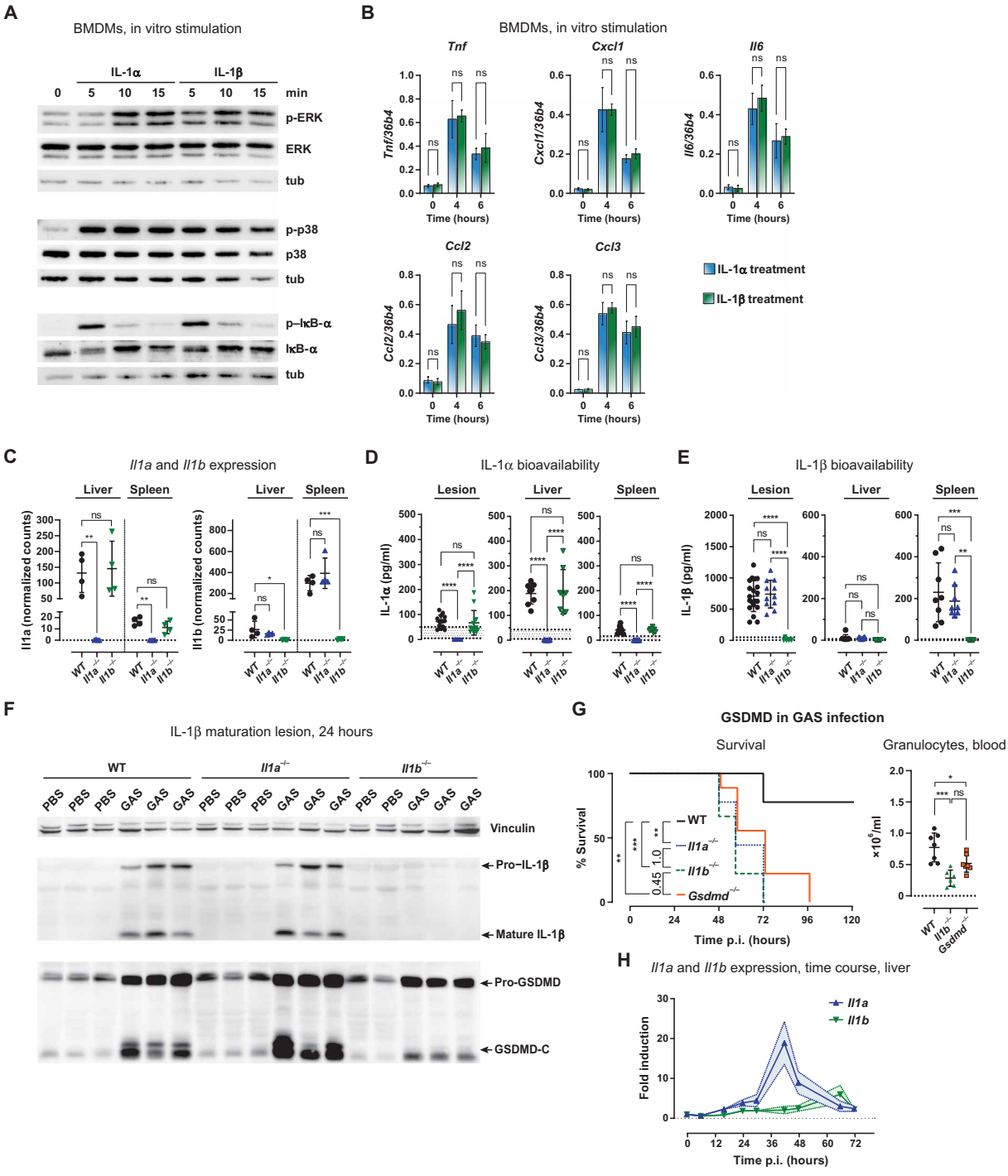

Fig. 7. Different local expressions of *Il1a* versus *Il1b* determine their distinct effects in organs during infection. (**A**) Signaling induced by IL-1α and IL-1β in WT BMDMs analyzed by Western blotting using antibodies for phosphorylated ERK (p-ERK), p38–MAP kinase (p-p38), and IκB-α (p–IκB-α), and for respective total protein as loading control. (**B**) Induction of *Tnf*, *Cxcl1*, *Il6*, *Ccl2*, and *Ccl3* by IL-1α or IL-1β in WT BMDMs analyzed by RT-qPCR. Student's *t* test, $n = 12$. (**C**) *Il1a* (left) and *Il1b* (right) expression (normalized counts) in livers and spleens from $Il1a^{-/-}$, $Il1b^{-/-}$, and WT mice 24 hours p.i. determined by RNA-seq. Counts in respective knockouts represent controls. Wald test from DESeq2, means with SDs, ***Padj < 0.001; **Padj < 0.01; *Padj < 0.05, not significant. (**D** and **E**) IL-1α (D) and IL-1β (E) protein levels in indicated tissues from $Il1a^{-/-}$, $Il1b^{-/-}$, and WT mice 24 hours p.i. determined in homogenates using ELISA, after normalization to total protein amounts. Student's *t* test, $n = 8$ per genotype. $^{**}P < 0.001$; $^{***}P < 0.0001$; $^{****}P < 0.00001$. (**F**) Lesion homogenates from GAS-infected or PBS-treated WT, $Il1a^{-/-}$, and $Il1b^{-/-}$ mice analyzed 24 hours p.i. by Western blotting using IL-1β and GSDMD antibodies. Loading control: vinculin. Each replicate represents a different mouse. (**G**) $Il1a^{-/-}$, $Il1b^{-/-}$, $Gsdmd^{-/-}$, and WT mice were infected with GAS and Kaplan-Meier survival curves (left; $n = 9$ per genotype, log-rank Mantel-Cox test with Bonferroni correction for multiple comparisons) and blood granulocyte counts 24 hours p.i. (right; $n = 6$ to 7 per genotype, one-way ANOVA with Tukey's test for multiple comparisons). ***$P > 0.001$; **$P > 0.01$; *$P > 0.05$. (**H**) Time course of *Il1a* and *Il1b* expression in the liver during GAS infection. Means of RT-qPCR data with the SE of median as area, $n = 4$ mice, each measured in duplicates.

IL-1β. Instead, our data indicate that these effects are a consequence of tissue-specific mRNA expression and, consistently, protein levels and bioavailability of these cytokines.

Distinct roles and tissue expression of *Il1a* versus *Il1b* during lung infection with *S. pneumoniae*

To address the distinct functions and expression patterns of *Il1a* versus *Il1b* in a different infection model, we used lung infection with *S. pneumoniae*. Similar to infection with GAS, *Il1a* and *Il1b* were each required for mouse protection (Fig. 8A). Moreover, *Il1b* prevented pathogen dissemination and promoted neutrophilia during lung infection (Fig. 8, B and C). In contrast, *Il1a* was dispensable for containment of bacteria and for neutrophilia (Fig. 8, B and C). Analysis of *Il1a* and *Il1b* expression revealed induction of both cytokines in the lung 48 and 72 hours p.i. (Fig. 8, B and C). However, *Il1a* was induced also in the spleen, whereas *Il1b* remained at the basal level in this organ; conversely, *Il1b*, not *Il1a*, was induced in the spleen (Fig. 8, B and C). Collectively, the effects of *Il1a* versus *Il1b* deficiencies and the differences in *Il1a* versus *Il1b* expression in organs during lung infection with *S. pneumoniae* resemble the findings we obtained for GAS infection. Thus, our model proposing that the nonredundancy of *Il1a* and *Il1b* in host defense is defined by distinct induction of these cytokines in tissues is probably relevant in other infections.

DISCUSSION

IL-1α and IL-1β induce comparable inflammatory responses in cells but are not redundant at the organismal level. Mechanistic models explaining the nonredundancy of *Il1a* and *Il1b* are not well developed. In this study, we used defined genetic models to describe distinct functions of *Il1a* and *Il1b* in host defense against GAS and mechanistically explain the nonredundancy of *Il1a* and *Il1b*. The vital role of IL-1 signaling in protection against GAS infections is supported by a high incidence of various types of invasive GAS diseases in patients receiving anti–IL-1–directed therapy (*43*).

Il1r1$^{-/-}$ mice exhibited a more severe course of the GAS disease than *Il1a*$^{-/-}$ and *Il1b*$^{-/-}$ mice as evident from the survival curves, larger necrotic areas at the site of infection and higher bacterial burden in one of the analyzed organs, i.e., the spleen. It is likely that the deficiency in responses to both IL-1α of IL-1β was causative of the more severe disease observed in *Il1r1*$^{-/-}$ mice. An involvement

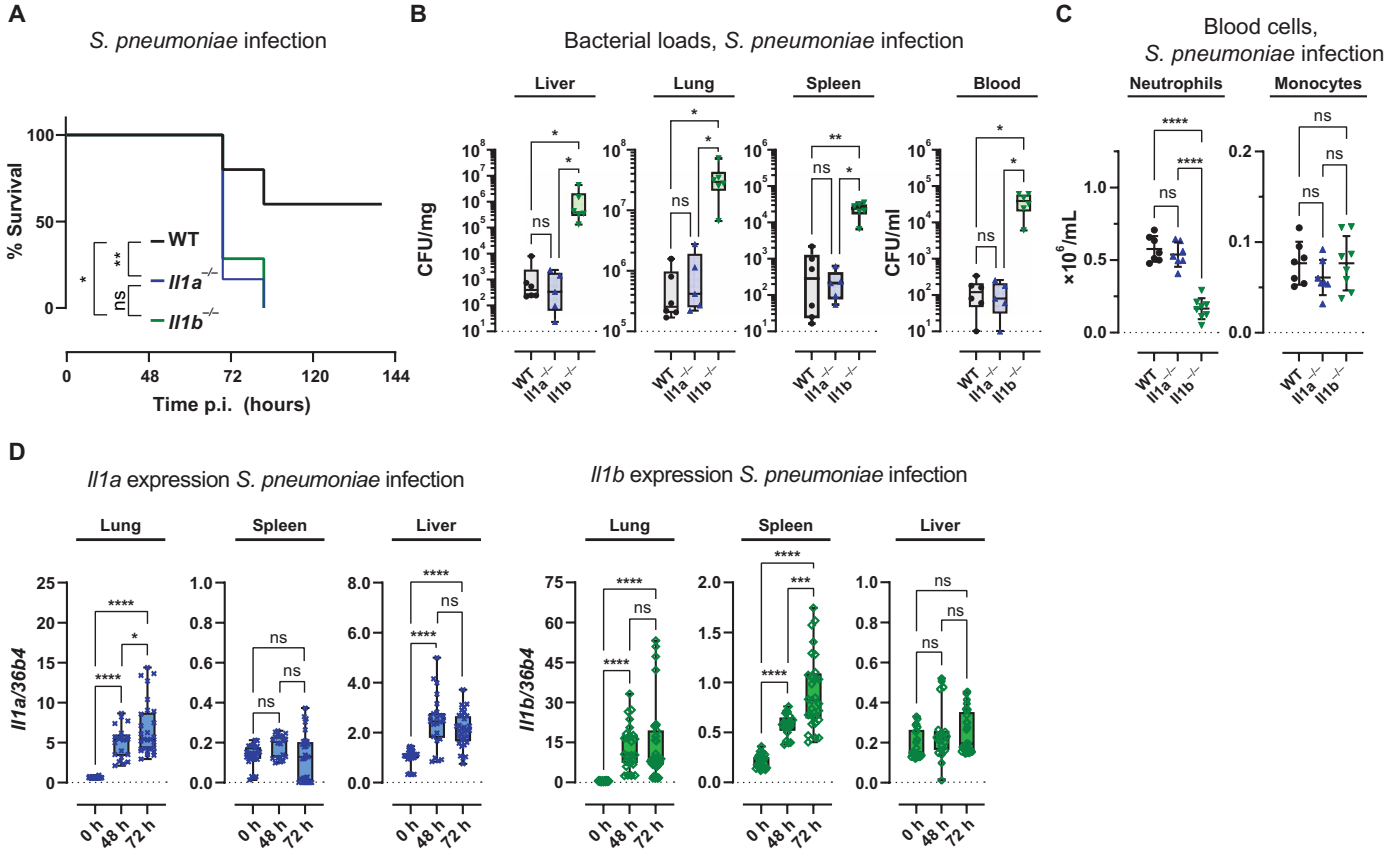

Fig. 8. Requirement for *Il1a* and *Il1b* during lung infection with *S. pneumonia*. (**A**) Kaplan-Meier survival curves for of *Il1a*$^{-/-}$, *Il1b*$^{-/-}$, and WT mice ($n = 7$ per genotype) infected intranasally with *S. pneumoniae*. Log-rank Mantel-Cox test. *$P < 0.05$; **$P < 0.01$. (**B**) Bacterial loads determined as CFUs in the lung, liver, spleen, and blood from *Il1a*$^{-/-}$, *Il1b*$^{-/-}$, and WT mice ($n = 6$ per genotype) 72 hours p.i. with *S. pneumonia*. The values represent CFUs per milliliter of blood or CFUs per gram total protein concentration of homogenized organ. Kruskal-Wallis with Dunn's multiple comparisons (all data points, median and 10th to 90th percentile shown). *$P < 0.05$; **$P < 0.01$. (**C**) Numbers of neutrophils (CD45$^+$ CD11b$^+$ Ly6C^{med} Ly6G$^+$) and monocytes (CD45$^+$ CD11b$^+$ Ly6G$^-$ Ly6C^{hi}) in the blood from *Il1a*$^{-/-}$, *Il1b*$^{-/-}$, and WT mice 72 hours p.i. ANOVA with Tukey's multiple comparisons test, $n = 7$. ****$P < 0.0001$. (**D**) Expression of *Il1a* or *Il1b* in the lung, spleen, and liver in WT animals 0, 48, and 72 hours p.i. Expression was normalized to the housekeeping gene *36b4*. Data are presented with the 10th to 90th percentile, and all data points are shown. ANOVA with Tukey's multiple comparison test, $n = 24$. ****$P < 0.0001$; ***$P < 0.001$; *$P < 0.05$.

of other IL-1R ligands such as the IL-1R antagonist IL-1RA cannot be excluded. Thus, the *Il1r1*$^{-/-}$ data cannot be deconvoluted to visualize the individual functions of *Il1a* or *Il1b*; instead, the results highlight the importance of a direct comparison of *Il1a*$^{-/-}$ mice with *Il1b*$^{-/-}$ mice for understanding the individual functions of IL-1α and IL-1β.

Protection against infectious diseases is driven by both resistance and tolerance (*44*, *45*). Resistance is caused by mechanisms that eliminate the invading pathogen, e.g., phagocytosis. Tolerance mechanisms do not target the pathogen but rather activate a complex repertoire of host responses that limit tissue damage and restore homeostatic conditions (*46*). From our infection experiments, it can be inferred that *Il1b* fosters resistance since the ability of *Il1b*$^{-/-}$ mice to clear the pathogen is markedly reduced. In contrast, *Il1a*$^{-/-}$ mice exhibit a regular pathogen clearance implying an essential role of *Il1a* in tolerance.

The beneficial activity of *Il1b* in resistance was apparent from higher bacterial loads in organs of *Il1b*$^{-/-}$ mice when compared to *Il1a*$^{-/-}$ and WT mice. An exception was the lesion that did not exhibit higher bacterial counts in *Il1b*$^{-/-}$ mice. This indicated that the pathogen was rapidly spreading from the primary site of infection to distant tissues in these mice, consistent with invasion of deeper tissues compared to *Il1a*$^{-/-}$ and WT mice. The deficiency in preventing dissemination and clearance of bacteria in *Il1b*$^{-/-}$ mice was associated with impaired neutrophil infiltration. The numbers of the infiltrating neutrophils are decisive for defeating GAS infection as illustrated in genetic models of enhanced neutrophilia (*24*, *28*). This suggests that the primary cause of the impaired bacterial clearance in *Il1b*$^{-/-}$ mice is a deficient deployment of neutrophils. In support of this, phagocytosis of GAS by neutrophils was not affected in *Il1b*$^{-/-}$ mice in vivo. However, selective effects of *Il1b* on other neutrophil antimicrobial functions cannot be excluded given that in vitro treatment of neutrophils by IL-1β was found to augment antimicrobial peptide expression but not oxidative burst (*47*).

Infection boosts the neutrophil production several-fold over the steady-state level by activation of emergency granulopoiesis in the BM (*48*). Emergency granulopoieses covers the higher demand for neutrophils during infection. Activation of emergency granulopoiesis during sterile immunostimulation with alum or polyinosinic:polycytidylic acid and upon infection of the oral cavity with *Candida albicans* is dependent on *Il1r1*, but the individual contributions of *Il1a* and *Il1b* remained unknown (*24*, *29*, *49*). Our finding that *Il1b*$^{-/-}$, but not *Il1a*$^{-/-}$, mice fail to launch emergency granulopoiesis establishes *Il1b* as specific driver of GAS-stimulated neutrophilia. Furthermore, our experiments using lung infection with *S. pneumoniae* imply that the function of *Il1b* as inducer of neutrophil production is not restricted to GAS infection. IL-1β cytokine was reported to promote HSC differentiation into GMPs in vitro (*24*, *29*, *50*). Nevertheless, IL-1β is not likely to directly stimulate granulopoiesis in vivo since *Il1r1*-dependent reactive neutrophilia requires the expression of *Il1r1* on radiation-resistant but not hematopoietic cells (*29*). A direct driver of emergency granulopoiesis is *Csf3*, which is known to be produced by various nonhematopoietic cells including endothelial cells during oral infection with *C. albicans* (*32*, *34*, *49*, *51*). The induction of endothelial *Csf3* in the oral cavity by *C. albicans* is dependent on *Il1r1* (*49*). Our current study identifies *Il1b*, not *Il1a*, as specific inducer of *Csf3*. The GAS-driven *Csf3* expression was observed in the lesion but not in the BM and spleen. This suggested that the *Csf3* source were nonhematopoietic cells. We speculate that *Csf3* originated from the muscle tissue present in the analyzed lesion since muscle cells were reported as substantial *Csf3* producers (*34*). An increase in levels of Csf3 protein (G-CSF) through exogenous administration phenocopies physiological emergency granulopoiesis (*51*). Thus, we propose that *Il1b* induces *Csf3* expression, which, in turn, drives emergency granulopoiesis during invasive infection with GAS.

Il1a is the major driver of GAS infection–induced liver adaptation as revealed by our RNA-seq experiments. The liver is the central metabolic hub, and adjustments in liver metabolism are indispensable for infectious disease tolerance, hence host survival (*52*). Adaptations of the hepatic metabolism to infection cues are readily detected in RNA-seq experiments of the whole liver because hepatocytes are the most abundant liver cells: The ratio of hepatocytes to Kupffer cells, the second most abundant liver cell type, is approximately 4:1 in mice (*37*, *53*). The analysis of the whole liver by RNA-seq is superior to the analysis of hepatocytes since these cells undergo rapid and extensive metabolic changes during isolation and in vitro culture (*54*). Our RNA-seq analysis unraveled the failure of *Il1a*$^{-/-}$ mice to induce a number of metabolic pathways including those regulating fatty acid, amino acid, and carbohydrate metabolism; these pathways were previously shown to be involved in context-dependent and mechanistically distinct ways in tolerance to infection cues: (i) Triglyceride synthesis is crucial for tissue protection in models of polybacterial (cecal ligation and puncture) and influenza infections (*39*), (ii) glucose metabolism exhibits opposing effects on tolerance in models of bacterial versus viral inflammation (*38*), and (iii) amino acid metabolism prevents liver tissue damage in a model of lymphocytic choriomeningitis virus infection (*37*). These studies indicate that metabolism is adapted by the host in multiple ways. The complex effects of these adaptations on the physiology and host defense remain to be elucidated. Our data propose the directions of future research that will seek to delineate the contribution of the *Il1a*-dependent metabolic pathways to host defense. Given the marked effect of *Il1a* on multiple metabolic pathways, we anticipate that host protection will be influenced by a combined output of these metabolic adaptations. In particular, it will be critical to determine how the *Il1a*-dependent effects impinge on host tolerance.

Although cell type–specific expression of *Il1a* and *Il1b* has been previously demonstrated, its relevance has not been addressed in vivo (*55*, *56*). We propose that the distinct impacts of *Il1a* and *Il1b* on the tissue transcriptome are governed by their different expression in a given tissue. This model is supported by several lines of evidence. First, *Il1a* is more highly expressed in the liver than *Il1b*, consistent with the profound *Il1a*-dependent liver transcriptome reprogramming and relatively small effects of *Il1b* in this organ. Conversely, *Il1b*, not *Il1a*, is strongly expressed in the spleen, which is substantially regulated by *Il1b* but not *Il1a*. Second, the majority of the small group of *Il1b*-regulated genes in the liver is also *Il1a* dependent, implying that *Il1a* and *Il1b* trigger qualitatively similar responses. Third, we also noticed higher expression of *Il1b* than *Il1a* in the lesion consistent with the dependence of *Csf3* induction on *Il1b* in this tissue. Moreover, responses of hepatocytes and BMDMs to IL-1α and IL-1β treatment are indistinguishable, consistent with the general notion that ligation of the IL-1 receptor with either of the two cytokines triggers the same signaling pathway (*1*, *2*). The possibility that the difference between *Il1a*$^{-/-}$ and *Il1b*$^{-/-}$ transcriptomes in a given organ (i.e., liver or spleen) was an indirect consequence of a

different course of infection in *Il1a*$^{-/-}$ and *Il1b*$^{-/-}$ mice is not supported by our data: The liver damage markers bilirubin and AST/ALT ratio were comparable in *Il1a*$^{-/-}$, *Il1b*$^{-/-}$, and WT mice. Moreover, the differences in, e.g., liver transcriptomes from *Il1a*$^{-/-}$ and *Il1b*$^{-/-}$ mice correlate with the expression profile of *Il1a* versus *Il1b* in the liver of WT animals, i.e., animals not perturbed by the lack of either *Il1a* or *Il1b*. We observed similar differences in *Il1a* versus *Il1b* expression in a different infection model, i.e., pneumonia caused by *S. pneumoniae*. Given that most of the few genes that are *Il1b* dependent in the liver are found in the *Il1a*-dependent group, we argue that the different effects of *Il1a* versus *Il1b* in the liver are a consequence of different levels of these cytokines in this organ rather than an indirect effect of divergent course of the disease in the respective knockout mice. However, a role of a different pathogenesis of infection in *Il1a*$^{-/-}$ and *Il1b*$^{-/-}$ mice in the organ-specific effects of *Il1a* and *Il1b* deficiencies cannot be ruled out.

Our study demonstrates that the biological activity of IL-1α and IL-1β is largely confined to the tissue of their mRNA expression. IL-1α activity is determined largely by protein levels since IL-1α can trigger the IL-1 receptor in the unprocessed form as a secreted or membrane-bound alarmin (*18*). IL-1β activity is determined by processing of pro–IL-1β into IL-1β, which is known to be efficient during GAS infection owing to activation of the NLR family pyrin domain containing 3 (NLRP3) inflammasome (*12*, *57*). In agreement, our study shows efficient maturation of pro–IL-1β to IL-1β in the infected tissue. The release of mature IL-1β during pyroptosis is dependent on GSDMD (*41*, *42*). The involvement of pyroptosis and GSDMD in IL-1β production during GAS infection is supported by our findings showing the requirement for GSDMD for host defense, containment of bacteria and reactive granulopoiesis. The susceptibility of *Gsdmd*$^{-/-}$ mice to GAS infection was less severe as compared to *Il1b*$^{-/-}$ mice, suggesting that IL-1β production was not entirely dependent on GSDMD. IL-1β that is generated independently of GSDMD possibly originates from cleavage of pro–IL-1β by the GAS-secreted protease SpeB, which is known to significantly contribute to IL-1β production during GAS infection (*43*). Our observation that *Gsdmd*$^{-/-}$ mice show a similar albeit less severe phenotype as compared to *Il1b*$^{-/-}$ mice suggests that GSDMD deficiency affects the function of *Il1b* but not *Il1a*. Moreover, functional impairment of both *Il1a* and *Il1b* in *Gsdmd*$^{-/-}$ mice would probably result in a more severe susceptibility, i.e., a phenotype resembling *Il1r1* deletion. However, a role of GSDMD in *Il1a* function cannot be excluded. Our data also show that IL-1α and IL-1β expressions (both mRNA and protein) are not mutually dependent on each other in any of the analyzed tissues. Furthermore, the data imply that IL-1α and IL-1β are unable to signal over long distances in vivo. This is likely to be caused by efficient sequestering of these cytokines by internalization and degradation of the ligated receptor (*58*). In the case of IL-1α, the local restriction of signaling can be facilitated by the membrane-bound pool of the incompletely processed cytokine, which is known to signal via direct cell-cell contacts (*59*).

In conclusion, the results of our study indicate that distinct functions of IL-1α versus IL-1β in host defense are defined by their different bioavailability relative to each other in a given tissue. The tissue-dependent ratios of IL-1α versus IL-1β levels result in dominant regulation of organs by one of the two cytokines. Given that organs have different roles in physiology, IL-1α and IL-1β acquire distinct functions: IL-1β drives resistance by inducing reactive granulopoiesis, while IL-1α orchestrates tolerance possibly through liver reprogramming. The results have broad physiological relevance, ranging from improved understanding of the nonredundancy of *Il1a* and *Il1b* to different regulations of resistance versus tolerance.

MATERIALS AND METHODS

Mice

Il1a$^{-/-}$, *Il1b*$^{-/-}$, *Il1r1*$^{-/-}$, and *Gsdmd*$^{-/-}$ mice have been described (*19*, *42*, *60*). All mice including WT mice were on C57BL/6 genetic background and regularly backcrossed. All mice were bred and housed under specific pathogen–free conditions with controlled temperature, humidity, a 12-hour light-dark regimen, as well as water and food ad libitum. Experiments were carried out using 7- to 11-week-old age- and sex-matched mice. This study was performed in accordance with the Austrian law for animal experiments and approved by the Austrian Ministry of Science under the license numbers BMWF-66.006/0019-WF/V/3b/2016 and BMWF-V/3b/2020-0.175.109.

GAS and *S. pneumoniae* cultures and infection of animals

GAS infection experiments were performed as described (*61*). GAS serotype M1 strain ISS3348 was used in all GAS infection experiments (*62*). Briefly, bacteria were grown at 37°C with 5% CO_2, without agitation in THY medium (Todd Hewitt broth from BD Biosciences, supplemented with 0.2% yeast extract; Sigma-Aldrich). Overnight cultures (stationary phase) were diluted 1:15 in THY medium, and after reaching optical density at 600 nm (OD_{600}) of 0.5 to 0.6 (mid-log phase), bacteria were harvested by centrifugation at 6000*g* for 8 min at 4°C and washed twice with cold sterile PBS. Last, bacteria were resuspended in 1:15 of the culture volume with isotonic saline (Sigma-Aldrich), resulting in 2×10^9 to 6×10^9 CFU/ml. For absolute CFU quantification, 50 µl of 10-fold serial dilutions in PBS were plated onto Columbia blood agar plates (Henry Schein). For infection, mice were anesthetized by intraperitoneal injection of ketamine (100 µg/g weight) (Ketamidor, Richter Pharma) and xylazine (10 µg/g weight) (Sedaxylan, Dechra). The fur of the upper left hind limb from anesthetized animals was shaved, and 50 µl (2×10^8 to 3×10^8 CFU) of freshly prepared bacterial suspension was injected subcutaneously in the region of the vastus lateralis. The health status of infected animals was monitored regularly and mice were euthanized when reaching predefined humane pathophysiological end points. Survival experiments were monitored for 5 days.

S. pneumoniae (American Type Culture Collection, 6303) (gift of S. Knapp) was grown in THY medium [3% (w/v) Todd Hewitt broth, supplemented with 0.2% (w/v) yeast extract] at 37°C with 5% CO_2 until reaching the stationary phase. Subsequently, cultures were diluted and incubated at 37°C with 5% CO_2 until reaching mid-log phase (OD_{600} = 0.4). Bacteria were pelleted (1000*g* for 15 min at 4°C), washed twice in PBS, and resuspended in PBS supplemented with 25% glycerol. Bacterial load was determined by plating serial 10-fold dilutions on Columbia agar plates containing 5% sheep blood (Henry Schein), and bacterial stocks were stored at −80°C. For lung infection, aliquots of frozen bacterial stocks were thawed and diluted in sterile PBS to 1×10^5 to 1.5×10^5 CFU/ml, as determined by plating 10-fold serial dilutions onto blood agar plates. Mice were anesthetized and infected intranasally with 30 µl of bacterial suspension. For survival, disease progression was monitored for 9 days, and mice were euthanized when reaching a humane end point.

Determination of bacterial dissemination and lesion size

At 24 hours p.i., the animals were deeply anesthetized [ketamine (150 μg/g) and xylazine (15 μg/g)], and precisely 500 of blood was withdrawn by vena cava puncture with a 25-gauge heparinized needle connected to a syringe containing 50 μl of heparin (100 U/ml; Sigma-Aldrich) to prevent coagulation and neutrophil activation. After euthanizing, the lesion, liver, spleen, kidney, and lung were isolated and disintegrated in ice-cold PBS with a rotor-stator homogenizer, and 10-fold dilution series were plated onto Columbia blood agar plates. Blood samples were diluted 1:2 in sterile double-distilled H_2O to lyse blood cells before serial dilution. Bacterial load was determined by CFU counting and normalization to volume (blood), tissue weight, or protein concentration (liver, lesion, spleen, and kidney). At 48 hours p.i., the width and length of the necrotic area (dark red– to black-colored skin) were measured and calculated as an elliptical area.

ELISA and hematologic counts and blood laboratory values

For cytokine measurements, tissue was homogenized in PBS containing protease inhibitor cocktail (cOmplete Roche), centrifuged for 10 min at 23,000*g*, and sterile-filtered. ELISAs were performed according to the manufacturer's protocols, and the results were normalized to total protein amount determined with BCA Pierce assay (Thermo Fisher Scientific). The organ damage markers urea, creatinine, AST, ALT, and GLDH were determined in heparinized plasma samples and analyzed by the veterinary in vitro diagnostics laboratory In Vitro GmbH. Hematologic counts were obtained using the V-Sight automated hematology analyzer (A. Menarini diagnostics). To assess bacteria-induced red blood cell rupture, free heme levels in plasma were measured. Heparinized blood from infected animals was centrifuged at 12,000*g* for 5 min at ambient temperature and diluted with H_2O in a 96-well plate (total volume, 100 μl), and heme concentration was determined by comparing to a hemin (Sigma-Aldrich) standard curve (0.25 to 16 μM in H_2O). For assessing the percentage of lysis, samples were compared to a standard curve of a dilution series made of the supernatant of completely lysed red blood cells diluted with H_2O. This supernatant was obtained by mixing 400 μl of heparinized blood with 14.5 ml of 0.1% sodium carbonate (Sigma-Aldrich) and incubation for 45 min at 37°C on a turning wheel, followed by centrifugation at 12,000*g* for 5 min. To each sample and standards, 150 μl of formic acid (Merck) was added, and absorbance was measured at 405 nm using a microplate reader.

Histology and immunohistochemistry

Infected mice were perfused at indicated time points by injecting 15 ml of ice-cold 4% paraformaldehyde (PFA) into the vena cava and at the same time cutting the hepatic portal vein. Tissue was removed, cut once longitudinally through the lesion or the large liver lobe, and fixed overnight in 4% PFA [in PBS (pH 6.9); Sigma-Aldrich). After dehydration and embedding in paraffin, 3-μm section was prepared. For hematoxylin and eosin (H&E) staining, a standardized routine protocol was applied. For CD45 and Ly6G staining, the antigen was retrieved by boiling for 10 min at 95°C in citrate buffer (10 mM; pH 6) or 10 min of proteinase K digestion (20 μg/ml in tris-EDTA; Sigma-Aldrich), respectively, followed by endogenous peroxidase blocking through incubation of deparaffinized and rehydrated slides in 3% H_2O_2 for 10 min. Blocking of unspecific antibody-binding was achieved with 3% mouse serum in tris-buffered saline with Tween 20 (TBS-T) and probed overnight at 4°C with primary rabbit anti-mouse CD45 (Cell Signaling Technology, #70257) or rat anti-mouse Ly6G (eBioscience, #14593182). Biotinylated secondary anti-rabbit or anti-rat antibodies (Vector Laboratories), respectively, were added and incubated at room temperature for 30 min, followed by adding biotin–horseradish peroxidase (HRP) conjugate (ABC-HRP kit, Vector laboratories) for 30 min at room temperature. Subsequently, slides were developed with chromogenic substrate 3,3′-diaminobenzidine (DAKO, Agilent) and counterstained with Harris hematoxylin (Merck). To stain GAS, deparaffinized and rehydrated slides were stained with nuclear fast red-aluminum solution (0.1%; Merck) for 8 min and counterstained with Gentian violet (Merck). To prevent background staining, slides were incubated with Lugol's solution (Merck) and rinsed with 96% ethanol. Images form dehydrated and in Eukitt (Sigma-Aldrich) mounted specimens were acquired with an Olympus slide scanner and processed with the supporting OlyVIA software (Olympus).

Scoring of histology sections

Consecutive skin sections stained with H&E, Gram, and Ly6G were scored for necrosis, bacterial invasion of the muscular layer, lack of colocalization of polymorphonuclear cells ($Ly6G^+$) and bacteria, and edema three times in a randomized and single-blind way. The reported values represent the median of the three individual scorings defined as 0 for no, 0.5 for minimal, 1 for mild, 1.5 for moderate, and 2 for severe effects. The values were combined to obtain the overall grading. Kruskal-Wallis with Dunn's multiple comparisons test was used for statistical evaluation.

RNA isolation and reverse transcription quantitative polymerase chain reaction

At the indicated time point, tissue was isolated from euthanized mice and homogenized in 1 ml of QIAzol Lysis Reagent (QIAGEN), followed by chloroform extraction. Total RNA was precipitated with a mixture of isopropanol and sodium chloride. cDNA was synthetized using a recombinant M-MuLV reverse transcriptase (RevertAid, Thermo Fisher Scientific) together with oligo$(dT)_{18}$ primer and used in reverse transcription quantitative polymerase chain reaction (RT-qPCR) with HOT FIREPol EvaGreen qPCR Supermix (Medibena) on CFX Touch qPCR cyclers (Bio-Rad) paired with CFX Maestro Analysis software. Relative expression levels were calculated by applying a twofold standard dilution series from cDNA derived from samples. The following primers were used: 36B4, TCCTTCTTCCAGGCTTTGGG (forward) and GGACACCCTCCAGAAAGCGA (reverse); Clc2, CTTCTGGGCCTGCTGTTCA (forward) and CCAGCCTACTCATTGGGATCA (reverse); Csf3, GCAGCCCAGATCACCCAGAAT (forward) and TGCAGGGCCATTAGCTTCAT (reverse); Elane, CTTCGAGAATGGCTTTGACC (forward) and CACATTGAGCTCTTGTAGCA (reverse); Il1a, CAAACTGATGAAGCTCGTCA (forward) and TCTCCTTGAGCGCTCACGAA (reverse); Il1b, TCTTTGAAGTTGACGGACCC (forward) and TGAGTGATACTGCCTGCCTG (reverse); Ptprc, TCATGGTCACACGATGTGAAGA (forward) and AGCCCGAGTGCCTTCCT (reverse); Tnf, GATCGGTCCCCAAAGGGATG (forward) and CACTTGGTGGTTTGCTACGAC (reverse); Il6, AGTTGCCTTCTTGGGACTGA (forward) and TTCTGCAAGTGCATCATCGT (reverse).

RNA sequencing

RNA was isolated as described above and DNA digestion was performed using deoxyribonuclease (DNase) (Roche) treatment for

30 min at 37°C. After RNA recovery with acidic phenol/chloroform/isoamyl alcohol (Ambion) extraction and ethanol precipitation, the quality was assessed using Agilent RNA 6000 Nano Assays (5067-1511) on an Agilent 2100 Bioanalyzer. Automated library preparation and multiplexing with the QuantSeq 3′ mRNA-seq Library Prep Kit (Lexogen), library-quality check, and sequencing on an Illumina HiSeqV4 SR50 platform with a read length of 50 bases were performed in the VBCF (Vienna BioCenter Core Facilities) Next Generation Sequencing (NGS) Facility (www.viennabiocenter.org/facilities). After demultiplexing by the facility, raw data were preprocessed (including quality control as well as barcode, adaptor, and quality trimming) using FastQC (www.bioinformatics.babraham.ac.uk/projects/fastqc/), mapped to the GRCm38/mm10 mouse genome assembly using STAR alignment version 2.5 and counted with HTSeq (version 0.11.) (*63*). Overall, each sample contained between 10 million and 15 million reads, of which, on average, 76% were uniquely mapped. Differential expression analysis was performed with obtained read counts using DESeq2 (V1.26.0) (*64*) with lfc shrinkage correction in R project version 3.6.1 with RStudio IDE version 1.0.143 (Foundation for Statistical Computing, Vienna, Austria, www.R-project.org/) (*65*). The raw data are accessible via the National Center for Biotechnology Information (NCBI)'s Gene Expression Omnibus (GEO) database under www.ncbi.nlm.nih.gov/geo/query/acc.cgi?acc=GSE167874 and the secure token krktocyqlnoxlcv.

Gene set enrichment analysis

For GSEA, normalized read counts of genes with significantly higher expression levels ([lfc > 1, false discovery rate < 0.05) between infected *Il1a*$^{-/-}$ and infected WT samples were used. Enrichment of GO biological processes was assessed with the GSEA desktop software (V4.0.3) and the MSigDB (V7.0) gene set database. Significantly enriched GO terms [|normalized enrichment score| (NES) > 1.5, $P < 0.01$] were visualized using the Enrichment Map plug-in (V1.1.0) for Cytoscape (V3.8.2) and grouped using the AutoAnnotate function. Heatmaps of selected AutoAnnotate clusters were generated with a z score (z score = sign (lfc) · − $\log_{10}(P_{adj})$ for |lfc| > 1 and $z = 1$ for |lfc|<1) between the indicated genotypes and the color range globally scored.

Preparation of single-cell suspensions for flow cytometry

Lesion

The lesion tissue was taken from euthanized mice, minced into small pieces, and incubated for 1 hour at 37°C with agitation in 5 ml of Dulbecco's modified Eagle's medium (DMEM) supplemented with collagenase-1 (1.5 mg/ml; Worthington), DNase-1 (0.4 mg/ml; Roche), and 0.5 mM $CaCl_2$. Digestion was stopped by adding 10 ml of PBS with 5 mM EDTA and 2% bovine serum albumin (BSA), and cell suspension was passed through a 70-μm cell strainer to obtain single cells.

Bone marrow

Femur and tibia of the noninfected hind leg were cut open at one end, transferred into a 1-ml tube with a hole at the bottom, and subsequently placed into a 1.5-ml centrifugation tube. Cells were obtained after a brief centrifugation step at 3000*g* for 30 s.

Spleen

Isolated spleens were homogenized through a 45-μm cell strainer with a 2-ml syringe plunger. Independent of the isolation method, red blood cells were lysed using a hypotonic ACK buffer (ammonium-chloride-potassium) and then washed twice with PBS.

Flow cytometry

To exclude dead cells, single-cell suspension was stained with Fixable Viability Dye eFluor 450 or eFluor 780 (eBioscience, Thermo Fisher Scientific), before blocking the FcγII/III receptor with an anti-CD16/anti-CD32 antibody (BioLegend). For staining of hematopoietic progenitor cells, no Fcγ block was performed; instead, cells were incubated with biotinylated antibody mixture from the lineage cell detection cocktail (Miltenyi), followed by staining with streptavidin–fluorescein isothiocyanate (FITC) conjugate (eBioscience, Thermo Fisher Scientific). For cell surface marker, an appropriate combination (as indicated in the figure legends) of antibodies conjugates was used and acquired with a BD LSR Fortessa flow cytometer. Debris and cell doublets were excluded based on the signal ratio of the forward scatter height/area as well as side scatter height/area and dead cells with the fluorescence of the viability dye. For blood samples, 15 μl of heparinized blood were mixed with 100 μl of fluorescence-activated cell sorting buffer and 25-μl containing beads (CountBright Absolute Counting Beads, Thermo Fisher Scientific). After centrifugation and washing, cells were stained with 25 μl of antibody mix including the viability dye and Fcγ block. Subsequently, cells were fixed with 4% PFA (Sigma-Aldrich) for 10 min, and red blood cells were lysed with ACK buffer. Antibody conjugates used are as follows(specificity, conjugate, clone, supplier, and catalog no.): CD11b, BV605, M1/70, BD Biosciences 563015; CD11b, PE-Cy7, M1/70, BD Biosciences 561098; CD16/32, PE93, eBioscience (Thermo Fisher Scientific), 12-0161-82; CD3, PE-CF594, 145-2C11, BD Biosciences 562286; CD34 APC, HM34, BioLegend, 128611; CD45, BV421, 30-F11, eBioscience (Thermo Fisher Scientific), 48-0451.82; c-Kit (CD117), BV711, 2B8, BD Biosciences 563160; Ly6C, PerCP-Cy7, HK1.4, eBioscience (Thermo Fisher Scientific), 45-5932-82; Ly6G, PE, 1A8, BioLegend, 127608; Ly6G, FITC, 1A8, BD Biosciences 551460, Sca-1 (Ly6A/E), PE-Cy7, D7, BD Biosciences 561021; Fcγ Block, TrueStain, 93, BioLegend, 101320; Fixable Viability Dye, eFluor 780, eBioscience (Thermo Fisher Scientific), 65-0865-14; Fixable Viability Dye, eFluor 450, eBioscience (Thermo Fisher Scientific), 65-0863-14; Lineage Cocktail, Biotin, Miltenyi, 130-092-613; Streptavidin, FITC, eBioscience (Thermo Fisher Scientific), 11-4317-87.

Peritonitis model and in vivo phagocytosis assay

Mid-log phase grown GAS cells were washed twice with sterile PBS, incubated for 30 min at 70°C to obtain heat-killed (HK) bacteria that were diluted in physiological NaCl (0.9%, B. Braun) and injected (2×10^8 CFU) into the peritoneum. After 24 hours, mice were euthanized, peritoneal cavity was flushed with 8 ml of PBS containing 0.02% EDTA, and the obtained cells in the extrudate were analyzed by flow cytometry. For in vivo phagocytosis assay, mice were first primed with intraperitoneal injection of HK bacteria for 16 hours to facilitate neutrophil recruitment. Subsequently, mice were injected with pHrodo Red, SE (Thermo Fisher Scientific)–stained HK GAS after labelling according to the manufacturer's protocol [pHrodo (20 ng/ml) for 1×10^8 bacteria/ml]. After 2 hours, the peritoneal extrudate was collected and stained, and phagocytic efficiency was calculated as counts of pHrodo$^+$ neutrophils normalized to the total number of counted neutrophils.

Primary cells and in vitro stimulation

Bone marrow–derived macrophages

BMDMs were differentiated from BM isolated from the lower limb bones of 7- to 9-weeks old mice with colony-stimulating factor-1 (derived from L929-cells) in DMEM (Sigma-Aldrich) supplemented

with 10% fetal bovine serum (FBS) (Sigma-Aldrich), streptomycin (100 μg/ml) (Sigma-Aldrich), and penicillin (100 U/ml) (Sigma-Aldrich) for 8 days.

Primary murine hepatocytes

WT mice were deeply anaesthetized [ketamine (150 μg/g) and xylazine (15 μg/g)] and the vena cava inferior cannulated (22G Venflon, BD) in its infrarenal region. After reassuring correct positioning, the venflon was fixed with a surgical suture (USP 5-0 SILON, Vitrex), the portal vein was punctured, and a clamp was placed onto the supradiaphragmatic vena cava inferior. Initially, the liver was perfused with 50 ml of Hanks' balanced salt solution (Gibco) containing 0.5 mM EDTA (Sigma-Aldrich) and heparin (120 U/ml) (Sigma-Aldrich), followed by in situ digestion with 20 ml of DMEM (Sigma-Aldrich) containing Liberase (40 mg/liter) (TM Research Grade, Roche, Sigma-Aldrich), both at a flow rate of 5 ml/min and prewarmed to 37°C. Subsequently, the liver was carefully isolated and placed in a petri dish, the gall bladder was removed, and the liver capsule was thoroughly ruptured with forceps. Obtained cell suspension was passed through a 100-μm cell strainer, filled up to 30 ml with William's E medium (Gibco, Thermo Fisher Scientific) containing 10% FBS, and centrifuged at 50*g* for 5 min at 4°C. Cell pellet was gently resuspended and washed twice with FBS-supplemented medium before plating in William's E medium (Gibco, Thermo Fisher Scientific) with 10% FBS, streptomycin (100 μg/ml; Sigma-Aldrich), penicillin (100 U/ml; Sigma-Aldrich), 5 mM L-glutamine (Sigma-Aldrich), and 1× nonessential amino acids on collagen-coated dishes. [For coating: type 1 collagen (0.1 mg/ml) in PBS for 24 hours at 4°C]. Hepatocytes were stimulated 24 hours after plating with recombinant mouse IL-1α (10 ng/ml) or rmIL-1β (10 ng/ml; PeproTech).

Peritoneal macrophages

The peritoneal cavities of CO_2-euthanized untreated mice were flushed with 5 to 6 ml of PBS containing 3% FBS. Obtained cell suspension was centrifuged with 500*g* for 10 min at 12°C, and 1.5×10^6 cells per well were seeded into a nontissue culture treated six-well plates. After 3 hours of incubation, all nonadherent cells were washed away, and cells were stimulated the next day with LPS (10 ng/ml; O55:B5, Sigma-Aldrich) for 9 hours. For inflammasome activation, additional 10 μM nigericin (Sigma-Aldrich) was added 2 hours before taking cell culture supernatant for subsequent ELISA measurements.

Western blotting

After stimulation, dishes were placed on ice and washed twice with ice-cold PBS, followed by scraping into cold Frackleton buffer [10 mM tris-HCl, 50 mM NaCl, 50 mM NaF, 30 mM $Na_4P_2O_7$, 1% Triton X-100, 1 mM dithiothreitol (DTT), 1 mM vanadate, and 1× protease inhibitor cocktail (cOmplete Roche)]. After five additional minutes on ice, the lysate was centrifuged at 13,000*g* for 5 min at 4°C, mixed at a ratio of 2:1 with SDS loading dye, and boiled for 5 min at 95°C. For lesion, tissue from infected or untreated mice was homogenized in 1 ml of PBS containing protease inhibitor cocktail and centrifuged with 3000*g* for 5 min at 4°C, and 400 μl of the obtained supernatant was mixed with 300 μl Fracelton buffer (without DTT), incubated 5 min on ice, and centrifuged with 21,000*g* for 5 min at 4°C. Protein concentration was adjusted after BCA (Thermo Fisher Scientific) measurement and mixed at a ratio 5:1 with a 6× SDS loading dye before boiling for 5 min at 95°C. SDS–polyacrylamide gel electrophoresis separation was performed with a 12% separation gel, and proteins were subsequently transferred to a nitrocellulose membrane (GE Healthcare) with the semidry method (Bio-Rad Trans-Blot Turbo) or for in vivo samples with the wet transfer method (Bio-Rad Trans-Blot cell). Next, the membrane was blocked with 5% BSA in TBS-T before probing overnight with primary antibody. The next day, the membrane was incubated with HRP-linked secondary antibody and SuperSignal West Chemiluminescent Substrate (Thermo Fisher Scientific; according to the manufacturer's protocol), followed by scanning using the ChemiDoc MP Imaging system (Bio-Rad). Antibodies for Western blot analyses were phosphorylated (p) p38, rabbit, Cell Signaling Technology, catalog no. 92115; p38, rabbit, Santa Cruz Biotechnology, catalog no. L0707; p–IκB-α, mouse, Cell Signaling Technology, catalog no. 9246; IκB-α, rabbit, Cell Signaling Technology, catalog no. 4812; p-ERK, rabbit, Cell Signaling Technology, catalog no. 9101; ERK, rabbit, Cell Signaling Technology, catalog no. 9012; IL-1β, goat, R&D Systems, catalog no. #AF401-NA; GSDMD, mouse, Santa Cruz Biotechnology, catalog no. sc-393581; Vinculin, mouse, Sigma-Aldrich, catalog no. #V9131; α-tubulin, mouse, Sigma-Aldrich, catalog no. T9026; Peroxidase AffiniPure Anti-Rabbit IgG (H + L), goat, Jackson ImmunoResearch, catalog no. 115-035-144; Peroxidase AffiniPure Anti-Mouse IgG (H + L), goat, Jackson ImmunoResearch, catalog no. 115-035-003.

Statistics

All visualizations and statistical analysis were performed using GraphPad Prism 9.0.0 or the R project. Statistical significances were calculated using an unpaired two-tailed Student's *t* test, one-way analysis of variance (ANOVA) with Bonferroni correction, Mann-Whitney *U* test, Kruskal-Wallis test, linear regression model, or Pearson's correlation tests, as indicated in the figure legends. Results were considered to be significant with $^*P < 0.05$, $^{**}P < 0.01$, and $^{***}P < 0.001$.

Ethics statement

Animal experiments were carried out according the Austrian law for animal experiments (BGBl. I Nr. 114/2012). Experiments were approved and authorized through the licenses BMWF-66.006/0019-WF/V/3b/2016 and BMWF-V/3b/2020-0.175.109 issued by the Austrian Ministry of Science and Research.

SUPPLEMENTARY MATERIALS

Supplementary material for this article is available at https://science.org/doi/10.1126/sciadv.abj7293

View/request a protocol for this paper from *Bio-protocol*.

REFERENCES AND NOTES

1. C. A. Dinarello, The IL-1 family of cytokines and receptors in rheumatic diseases. *Nat. Rev. Rheumatol.* **15**, 612–632 (2019).
2. A. Mantovani, C. A. Dinarello, M. Molgora, C. Garlanda, Interleukin-1 and related cytokines in the regulation of inflammation and immunity. *Immunity* **50**, 778–795 (2019).
3. C. A. Dinarello, Overview of the IL-1 family in innate inflammation and acquired immunity. *Immunol. Rev.* **281**, 8–27 (2018).
4. B. Krumm, Y. Xiang, J. Deng, Structural biology of the IL-1 superfamily: Key cytokines in the regulation of immune and inflammatory responses. *Protein Sci.* **23**, 526–538 (2014).
5. S. Moorlag, R. J. Roring, L. A. B. Joosten, M. G. Netea, The role of the interleukin-1 family in trained immunity. *Immunol. Rev.* **281**, 28–39 (2018).
6. Y. Zhang, S. Saccani, H. Shin, B. S. Nikolajczyk, Dynamic protein associations define two phases of IL-1β transcriptional activation. *J. Immunol.* **181**, 503–512 (2008).
7. N. Mori, D. Prager, Transactivation of the interleukin-1alpha promoter by human T-cell leukemia virus type I and type II Tax proteins. *Blood* **87**, 3410–3417 (1996).
8. K. Alheim, T. L. McDowell, J. A. Symons, G. W. Duff, T. Bartfai, An AP-1 site is involved in the NGF induction of IL-1α in PC12 cells. *Neurochem. Int.* **29**, 487–496 (1996).
9. S. Bailly, M. Fay, N. Israel, M. A. Gougerot-Pocidalo, The transcription factor AP-1 binds to the human interleukin 1 alpha promoter. *Eur. Cytokine Netw.* **7**, 125–128 (1996).

10. T. L. McDowell, J. A. Symons, G. W. Duff, Human interleukin-1α gene expression is regulated by Sp1 and a transcriptional repressor. *Cytokine* **30**, 141–153 (2005).
11. G. M. Tannahill, A. M. Curtis, J. Adamik, E. M. Palsson-McDermott, A. F. McGettrick, G. Goel, C. Frezza, N. J. Bernard, B. Kelly, N. H. Foley, L. Zheng, A. Gardet, Z. Tong, S. S. Jany, S. C. Corr, M. Haneklaus, B. E. Caffrey, K. Pierce, S. Walmsley, F. C. Beasley, E. Cummins, V. Nizet, M. Whyte, C. T. Taylor, H. Lin, S. L. Masters, E. Gottlieb, V. P. Kelly, C. Clish, P. E. Auron, R. J. Xavier, L. A. J. O'Neill, Succinate is an inflammatory signal that induces IL-1β through HIF-1α. *Nature* **496**, 238–242 (2013).
12. V. Castiglia, A. Piersigilli, F. Ebner, M. Janos, O. Goldmann, U. Damböck, A. Kröger, S. Weiss, S. Knapp, A. M. Jamieson, C. Kirschning, U. Kalinke, B. Strobl, M. Müller, D. Stoiber, S. Lienenklaus, P. Kovarik, Type I interferon signaling prevents IL-1β-driven lethal systemic hyperinflammation during invasive bacterial infection of soft tissue. *Cell Host Microbe* **19**, 375–387 (2016).
13. J. Lu, X. Wu, M. Hong, P. Tobias, J. Han, A potential suppressive effect of natural antisense IL-1β RNA on lipopolysaccharide-induced IL-1β expression. *J. Immunol.* **190**, 6570–6578 (2013).
14. J. P. Cogswell, M. M. Godlevski, G. B. Wisely, W. C. Clay, L. M. Leesnitzer, J. P. Ways, J. G. Gray, NF-kappa B regulates IL-1 beta transcription through a consensus NF-kappa B binding site and a nonconsensus CRE-like site. *J. Immunol.* **153**, 712–723 (1994).
15. L. Sneezum, K. Eislmayr, H. Dworak, V. Sedlyarov, A. le Heron, F. Ebner, I. Fischer, Y. Iwakura, P. Kovarik, Context-dependent IL-1 mRNA-destabilization by TTP prevents dysregulation of immune homeostasis under steady state conditions. *Front. Immunol.* **11**, 1398 (2020).
16. K. Schroder, T. D. Kanneganti, F. Shao, P. Broz, Mechanisms and consequences of inflammasome activation. *J. Mol. Biol.* **430**, 131–132 (2018).
17. V. A. K. Rathinam, Y. Zhao, F. Shao, Innate immunity to intracellular LPS. *Nat. Immunol.* **20**, 527–533 (2019).
18. A. Malik, T. D. Kanneganti, Function and regulation of IL-1α in inflammatory diseases and cancer. *Immunol. Rev.* **281**, 124–137 (2018).
19. R. Horai, M. Asano, K. Sudo, H. Kanuka, M. Suzuki, M. Nishihara, M. Takahashi, Y. Iwakura, Production of mice deficient in genes for interleukin (IL)-1α, IL-1β, IL-1α/β, and IL-1 receptor antagonist shows that IL-1β is crucial in turpentine-induced fever development and glucocorticoid secretion. *J. Exp. Med.* **187**, 1463–1475 (1998).
20. M. Sultan, Z. Ben-Ari, R. Masoud, O. Pappo, D. Harats, Y. Kamari, M. Safran, Interleukin-1α and Interleukin-1β play a central role in the pathogenesis of fulminant hepatic failure in mice. *PLOS ONE* **12**, e0184084 (2017).
21. M. Bersudsky, L. Luski, D. Fishman, R. M. White, N. Ziv-Sokolovskaya, S. Dotan, P. Rider, I. Kaplanov, T. Aychek, C. A. Dinarello, R. N. Apte, E. Voronov, Non-redundant properties of IL-1α and IL-1β during acute colon inflammation in mice. *Gut* **63**, 598–609 (2014).
22. K. D. Mayer-Barber, B. B. Andrade, D. L. Barber, S. Hieny, C. G. Feng, P. Caspar, S. Oland, S. Gordon, A. Sher, Innate and adaptive interferons suppress IL-1α and IL-1β production by distinct pulmonary myeloid subsets during *Mycobacterium tuberculosis* infection. *Immunity* **35**, 1023–1034 (2011).
23. K. C. Barry, M. F. Fontana, J. L. Portman, A. S. Dugan, R. E. Vance, IL-1α signaling initiates the inflammatory response to virulent *Legionella pneumophila* in vivo. *J. Immunol.* **190**, 6329–6339 (2013).
24. L. C. Hsu, T. Enzler, J. Seita, A. M. Timmer, C. Y. Lee, T. Y. Lai, G. Y. Yu, L. C. Lai, V. Temkin, U. Sinzig, T. Aung, V. Nizet, I. L. Weissman, M. Karin, IL-1β-driven neutrophilia preserves antibacterial defense in the absence of the kinase IKKβ. *Nat. Immunol.* **12**, 144–150 (2011).
25. G. Sierig, C. Cywes, M. R. Wessels, C. D. Ashbaugh, Cytotoxic effects of streptolysin o and streptolysin s enhance the virulence of poorly encapsulated group a streptococci. *Infect. Immun.* **71**, 446–455 (2003).
26. S. Dohrmann, J. N. Cole, V. Nizet, Conquering neutrophils. *PLOS Pathog.* **12**, e1005682 (2016).
27. A. S. Zinkernagel, A. M. Timmer, M. A. Pence, J. B. Locke, J. T. Buchanan, C. E. Turner, I. Mishalian, S. Sriskandan, E. Hanski, V. Nizet, The IL-8 protease SpyCEP/ScpC of group A *Streptococcus* promotes resistance to neutrophil killing. *Cell Host Microbe* **4**, 170–178 (2008).
28. F. Ebner, V. Sedlyarov, S. Tasciyan, M. Ivin, F. Kratochvill, N. Gratz, L. Kenner, A. Villunger, M. Sixt, P. Kovarik, The RNA-binding protein tristetraprolin schedules apoptosis of pathogen-engaged neutrophils during bacterial infection. *J. Clin. Invest.* **127**, 2051–2065 (2017).
29. Y. Ueda, D. W. Cain, M. Kuraoka, M. Kondo, G. Kelsoe, IL-1R type I-dependent hemopoietic stem cell proliferation is necessary for inflammatory granulopoiesis and reactive neutrophilia. *J. Immunol.* **182**, 6477–6484 (2009).
30. A. A. Navarini, K. S. Lang, A. Verschoor, M. Recher, A. S. Zinkernagel, V. Nizet, B. Odermatt, H. Hengartner, R. M. Zinkernagel, Innate immune-induced depletion of bone marrow neutrophils aggravates systemic bacterial infections. *Proc. Natl. Acad. Sci. U.S.A.* **106**, 7107–7112 (2009).
31. H. Iwasaki, K. Akashi, Myeloid lineage commitment from the hematopoietic stem cell. *Immunity* **26**, 726–740 (2007).
32. G. J. Lieschke, D. Grail, G. Hodgson, D. Metcalf, E. Stanley, C. Cheers, K. J. Fowler, S. Basu, Y. F. Zhan, A. R. Dunn, Mice lacking granulocyte colony-stimulating factor have chronic neutropenia, granulocyte and macrophage progenitor cell deficiency, and impaired neutrophil mobilization. *Blood* **84**, 1737–1746 (1994).
33. A. M. Ordelheide, N. Gommer, A. Böhm, C. Hermann, I. Thielker, F. Machicao, A. Fritsche, N. Stefan, H. U. Häring, H. Staiger, Granulocyte colony-stimulating factor (G-CSF): A saturated fatty acid-induced myokine with insulin-desensitizing properties in humans. *Mol. Metab.* **5**, 305–316 (2016).
34. H. Li, Q. Chen, C. Li, R. Zhong, Y. Zhao, Q. Zhang, W. Tong, D. Zhu, Y. Zhang, Muscle-secreted granulocyte colony-stimulating factor functions as metabolic niche factor ameliorating loss of muscle stem cells in aged mice. *EMBO J.* **38**, e102154 (2019).
35. N. Gehrke, N. Hövelmeyer, A. Waisman, B. K. Straub, J. Weinmann-Menke, M. A. Wörns, P. R. Galle, J. M. Schattenberg, Hepatocyte-specific deletion of IL1-RI attenuates liver injury by blocking IL-1 driven autoinflammation. *J. Hepatol.* **68**, 986–995 (2018).
36. I. K. Pang, T. Ichinohe, A. Iwasaki, IL-1R signaling in dendritic cells replaces pattern-recognition receptors in promoting $CD8^{+}$T cell responses to influenza A virus. *Nat. Immunol.* **14**, 246–253 (2013).
37. A. Lercher, A. Bhattacharya, A. M. Popa, M. Caldera, M. F. Schlapansky, H. Baazim, B. Agerer, B. Gürtl, L. Kosack, P. Májek, J. S. Brunner, D. Vitko, T. Pinter, J.-W. Genger, A. Orlova, N. Pikor, D. Reil, M. Ozsvár-Kozma, U. Kalinke, B. Ludewig, R. Moriggl, K. L. Bennett, J. Menche, P. N. Cheng, G. Schabbauer, M. Trauner, K. Klavins, A. Bergthaler, Type I interferon signaling disrupts the hepatic urea cycle and alters systemic metabolism to suppress T cell function. *Immunity* **51**, 1074–1087.e9 (2019).
38. A. Wang, S. C. Huen, H. H. Luan, S. Yu, C. Zhang, J.-D. Gallezot, C. J. Booth, R. Medzhitov, Opposing effects of fasting metabolism on tissue tolerance in bacterial and viral inflammation. *Cell* **166**, 1512–1525.e12 (2016).
39. H. H. Luan, A. Wang, B. K. Hilliard, F. Carvalho, C. E. Rosen, A. M. Ahasic, E. L. Herzog, I. Kang, M. A. Pisani, S. Yu, C. Zhang, A. M. Ring, L. H. Young, R. Medzhitov, GDF15 is an inflammation-induced central mediator of tissue tolerance. *Cell* **178**, 1231–1244.e11 (2019).
40. S. Freigang, F. Ampenberger, A. Weiss, T. D. Kanneganti, Y. Iwakura, M. Hersberger, M. Kopf, Fatty acid-induced mitochondrial uncoupling elicits inflammasome-independent IL-1α and sterile vascular inflammation in atherosclerosis. *Nat. Immunol.* **14**, 1045–1053 (2013).
41. J. Shi, Y. Zhao, K. Wang, X. Shi, Y. Wang, H. Huang, Y. Zhuang, T. Cai, F. Wang, F. Shao, Cleavage of GSDMD by inflammatory caspases determines pyroptotic cell death. *Nature* **526**, 660–665 (2015).
42. N. Kayagaki, I. B. Stowe, B. L. Lee, K. O'Rourke, K. Anderson, S. Warming, T. Cuellar, B. Haley, M. Roose-Girma, Q. T. Phung, P. S. Liu, J. R. Lill, H. Li, J. Wu, S. Kummerfeld, J. Zhang, W. P. Lee, S. J. Snipas, G. S. Salvesen, L. X. Morris, L. Fitzgerald, Y. Zhang, E. M. Bertram, C. C. Goodnow, V. M. Dixit, Caspase-11 cleaves gasdermin D for non-canonical inflammasome signalling. *Nature* **526**, 666–671 (2015).
43. C. N. LaRock, J. Todd, D. L. La Rock, J. Olson, A. J. O'Donoghue, A. A. B. Robertson, M. A. Cooper, H. M. Hoffman, V. Nizet, IL-1β is an innate immune sensor of microbial proteolysis. *Sci. Immunol.* **1**, eaah3539 (2016).
44. M. P. Soares, L. Teixeira, L. F. Moita, Disease tolerance and immunity in host protection against infection. *Nat. Rev. Immunol.* **17**, 83–96 (2017).
45. J. S. Ayres, D. S. Schneider, Tolerance of infections. *Annu. Rev. Immunol.* **30**, 271–294 (2012).
46. J. L. McCarville, J. S. Ayres, Disease tolerance: Concept and mechanisms. *Curr. Opin. Immunol.* **50**, 88–93 (2018).
47. O. Dmitrieva-Posocco, A. Dzutsev, D. F. Posocco, V. Hou, W. Yuan, V. Thovarai, I. A. Mufazalov, M. Gunzer, I. P. Shilovskiy, M. R. Khaitov, G. Trinchieri, A. Waisman, S. I. Grivennikov, Cell-type-specific responses to interleukin-1 control microbial invasion and tumor-elicited inflammation in colorectal cancer. *Immunity* **50**, 166–180.e7 (2019).
48. M. G. Manz, S. Boettcher, Emergency granulopoiesis. *Nat. Rev. Immunol.* **14**, 302–314 (2014).
49. S. Altmeier, A. Toska, F. Sparber, A. Teijeira, C. Halin, S. L. Gut-Landmann, IL-1 coordinates the neutrophil response to *C. albicans* in the oral mucosa. *PLOS Pathog.* **12**, e1005882 (2016).
50. E. M. Pietras, C. Mirantes-Barbeito, S. Fong, D. Loeffler, L. V. Kovtonyuk, S. Y. Zhang, R. Lakshminarasimhan, C. P. Chin, J. M. Techner, B. Will, C. Nerlov, U. Steidl, M. G. Manz, T. Schroeder, E. Passegué, Chronic interleukin-1 exposure drives haematopoietic stem cells towards precocious myeloid differentiation at the expense of self-renewal. *Nat. Cell Biol.* **18**, 607–618 (2016).
51. S. Boettcher, P. Ziegler, M. A. Schmid, H. Takizawa, N. van Rooijen, M. Kopf, M. Heikenwalder, M. G. Manz, Cutting edge: LPS-induced emergency myelopoiesis depends on TLR4-expressing nonhematopoietic cells. *J. Immunol.* **188**, 5824–5828 (2012).
52. K. Troha, J. S. Ayres, Metabolic adaptations to infections at the organismal level. *Trends Immunol.* **41**, 113–125 (2020).

53. B. G. Lopez, M. S. Tsai, J. L. Baratta, K. J. Longmuir, R. T. Robertson, Characterization of Kupffer cells in livers of developing mice. *Comp. Hepatol.* **10**, 2 (2011).
54. S. Cassim, V. A. Raymond, P. Lapierre, M. Bilodeau, From in vivo to in vitro: Major metabolic alterations take place in hepatocytes during and following isolation. *PLOS ONE* **12**, e0190366 (2017).
55. G. Chen, L. Sun, T. Kato, K. Okuda, M. B. Martino, A. Abzhanova, J. M. Lin, R. C. Gilmore, B. D. Batson, Y. K. O'Neal, A. S. Volmer, H. Dang, Y. Deng, S. H. Randell, B. Button, A. Livraghi-Butrico, M. Kesimer, C. M. P. Ribeiro, W. K. O'Neal, R. C. Boucher, IL-1β dominates the promucin secretory cytokine profile in cystic fibrosis. *J. Clin. Invest.* **129**, 4433–4450 (2019).
56. J. Lugrin, R. Parapanov, N. Rosenblatt-Velin, S. Rignault-Clerc, F. Feihl, B. Waeber, O. Müller, C. Vergely, M. Zeller, A. Tardivel, P. Schneider, P. Pacher, L. Liaudet, Cutting edge: IL-1α is a crucial danger signal triggering acute myocardial inflammation during myocardial infarction. *J. Immunol.* **194**, 499–503 (2015).
57. J. Harder, L. Franchi, R. Muñoz-Planillo, J. H. Park, T. Reimer, G. Núñez, Activation of the Nlrp3 inflammasome by *Streptococcus pyogenes* requires streptolysin O and NF-κB activation but proceeds independently of TLR signaling and P2X7 receptor. *J. Immunol.* **183**, 5823–5829 (2009).
58. S. B. Mizel, P. L. Kilian, J. C. Lewis, K. A. Paganelli, R. A. Chizzonite, The interleukin 1 receptor. Dynamics of interleukin 1 binding and internalization in T cells and fibroblasts. *J. Immunol.* **138**, 2906–2912 (1987).
59. J. N. E. Chan, M. Humphry, L. Kitt, D. Krzyzanska, K. J. Filbey, M. R. Bennett, M. C. H. Clarke, Cell surface IL-1α trafficking is specifically inhibited by interferon-γ, and associates with the membrane via IL-1R2 and GPI anchors. *Eur. J. Immunol.* **50**, 1663–1675 (2020).
60. M. Labow, D. Shuster, M. Zetterstrom, P. Nunes, R. Terry, E. B. Cullinan, T. Bartfai, C. Solorzano, L. L. Moldawer, R. Chizzonite, K. W. M. Intyre, Absence of IL-1 signaling and reduced inflammatory response in IL-1 type I receptor-deficient mice. *J. Immunol.* **159**, 2452–2461 (1997).
61. N. Gratz, H. Hartweger, U. Matt, F. Kratochvill, M. Janos, S. Sigel, B. Drobits, X. D. Li, S. Knapp, P. Kovarik, Type I interferon production induced by *Streptococcus pyogenes*-derived nucleic acids is required for host protection. *PLOS Pathog.* **7**, e1001345 (2011).
62. M. Mora, G. Bensi, S. Capo, F. Falugi, C. Zingaretti, A. G. O. Manetti, T. Maggi, A. R. Taddei, G. Grandi, J. L. Telford, Group A *Streptococcus* produce pilus-like structures containing protective antigens and Lancefield T antigens. *Proc. Natl. Acad. Sci. U.S.A.* **102**, 15641–15646 (2005).
63. S. Anders, P. T. Pyl, W. Huber, HTSeq—A Python framework to work with high-throughput sequencing data. 31, *Bioinformatics*, 166–Bioinformat169 (2015).
64. M. I. Love, W. Huber, S. Anders, Moderated estimation of fold change and dispersion for RNA-seq data with DESeq2. *Genome Biol.* **15**, 550 (2014).
65. R. C. Team, R: A Language and Environment for Statistical Computing (2017).

Acknowledgments: We thank R. Eferl, J. Schmid, and A. Bergthaler for helpful discussions. We are grateful to P. Berthold for animal husbandry. The VBCF NGS Facility (www.viennabiocenter.org/facilities) and L. Paul from Lexogen are acknowledged for sequencing advice. We thank A. LeHeron for critically reading the manuscript. **Funding:** Research in the Lamkanfi laboratory is supported by grants from the European Research Council (grant 683144) and the Fund for Scientific Research-Flanders (grants G014221N and G017121N). This work was supported by the Austrian Science Fund (FWF) grants P33000-B, P31848-B, and W1261 to P.K. and the University of Vienna uni:docs fellowship to M.B. **Author contributions:** Conceptualization: K.E. and P.K. Methodology: K.E., L.V.W., and M.L. Investigation: K.E., A.B., L.M., and M.B. Figures: K.E. Supervision: P.K., K.E., and M.L. Writing: K.E. and P.K. **Competing interests:** The authors declare they have no competing interests. **Data and materials availability:** All raw RNA-seq data are accessible via the NCBI's GEO under the accession number GSE167874. Gsdmd$^{-/-}$ mice can be provided by Genentech Inc., Il1a$^{-/-}$ and Il1b$^{-/-}$ mice can be provided by Y. Iwakura, Tokyo University of Science, pending scientific review and a completed material transfer agreement. Requests for the Gsdmd$^{-/-}$, Il1a$^{-/-}$, or Il1b$^{-/-}$ should be submitted to Genentech Inc. and Y. Iwakura, Tokyo University of Science, respectively. All data needed to evaluate the conclusions in the paper are present in the paper and/or the Supplementary Materials.

Submitted 28 May 2021
Accepted 5 January 2022
Published 2 March 2022
10.1126/sciadv.abj7293